Journal of Hydrology 558 (2018) 632–646

Contents lists available at ScienceDirect

Journal of Hydrology

journal homepage: www.elsevier.com/locate/jhydrol

Research papers

# Reconstructing pre-instrumental streamflow in Eastern Australia using a water balance approach

C.R. Tozer [a,*], A.S. Kiem [b], T.R. Vance [c], J.L. Roberts [d,c], M.A.J. Curran [d,c], A.D. Moy [d,c]

[a] Oceans & Atmosphere, CSIRO, Castray Esplanade, Hobart, Tasmania 7000, Australia
[b] Centre for Water, Climate and Land (CWCL), University of Newcastle, Callaghan, NSW 2308, Australia
[c] Antarctic Climate & Ecosystems Cooperative Research Centre, University of Tasmania, Private Bag 80, Hobart, Tasmania 7001, Australia
[d] Australian Antarctic Division, Kingston, Tasmania 7050, Australia

ARTICLE INFO

*Article history:*
Received 31 July 2017
Received in revised form 4 January 2018
Accepted 31 January 2018
Available online 15 February 2018
This manuscript was handled by Marco Borga, Editor-in-Chief, with the assistance of Daqing Yang, Associate Editor

*Keywords:*
Drought
Floods
Streamflow
Reconstruction
Paleoclimate
Budyko

ABSTRACT

Streamflow reconstructions based on paleoclimate proxies provide much longer records than the short instrumental period records on which water resource management plans are currently based. In Australia there is a lack of in-situ high resolution paleoclimate proxy records, but remote proxies with teleconnections to Australian climate have utility in producing streamflow reconstructions. Here we investigate, via a case study for a catchment in eastern Australia, the novel use of an Antarctic ice-core based rainfall reconstruction within a Budyko-framework to reconstruct ~1000 years of annual streamflow. The resulting streamflow reconstruction captures interannual to decadal variability in the instrumental streamflow, validating both the use of the ice core rainfall proxy record and the Budyko-framework method. In the preinstrumental era the streamflow reconstruction shows longer wet and dry epochs and periods of streamflow variability that are higher than observed in the instrumental era. Importantly, for both the instrumental record and preinstrumental reconstructions, the wet (dry) epochs in the rainfall record are shorter (longer) in the streamflow record and this non-linearity must be considered when inferring hydroclimatic risk or historical water availability directly from rainfall proxy records alone. These insights provide a better understanding of present infrastructure vulnerability in the context of past climate variability for eastern Australia. The streamflow reconstruction presented here also provides a better understanding of the range of hydroclimatic variability possible, and therefore represents a more realistic baseline on which to quantify the potential impacts of anthropogenic climate change on water security.

© 2018 Elsevier B.V. All rights reserved.

## 1. Introduction

Rainfall and streamflow reconstructions from paleoclimate proxies indicate that the instrumental climate record does not capture the full range of climate variability (e.g. Meko et al., 1995; Cook et al., 1999; Woodhouse and Lukas, 2006a,b; Allen et al., 2015b; Vance et al., 2015; Ho et al., 2016; Tozer et al., 2016). Importantly, Thyer et al. (2009) showed that instrumental climate records, on which water resource management plans are based, produce high parameter uncertainty in stochastic models and that longer records are required to reduce uncertainty and enable proper stochastic model identification. Where paleoclimate data is used, longer wet and dry sequences are observed, allowing for the development of more realistic statistics on which to design water infrastructure and develop catchment management plans (Biondi et al., 2002; Verdon and Franks, 2007; Biondi et al., 2008; Prairie et al., 2008; Henley et al., 2011; Patskoski and Sankarasubramanian, 2015). As such, researchers are investigating the incorporation of paleoclimate reconstructions, and more specifically, streamflow reconstructions, into water management and planning (e.g. Thyer et al., 2006; Woodhouse and Lukas, 2006b; Prairie et al., 2008; Patskoski and Sankarasubramanian, 2015). However, knowledge gaps still exist and, in practice, the uptake of insights from paleoclimate research remains limited, especially in Australia where water resources management is primarily based on short (~100 years at best) instrumental rainfall and streamflow records (e.g. Kiem et al., 2016).

High resolution streamflow reconstructions are traditionally developed from tree ring records given their high temporal resolution and ability to represent local hydroclimatic behaviour (Elshorbagy et al., 2016; Razavi et al., 2016). In North America, a

* Corresponding author.
*E-mail address:* carly.tozer@csiro.au (C.R. Tozer).

https://doi.org/10.1016/j.jhydrol.2018.01.064
0022-1694/© 2018 Elsevier B.V. All rights reserved.

broad network of tree ring records (see Fig. 5 in Cook et al. (2010)) has afforded the development of numerous streamflow reconstructions in water catchments across the region (e.g. Meko et al., 1995; Meko et al., 2001; Woodhouse and Lukas, 2006a,b; Ho et al., 2016). In Australia, however, there is a lack of in situ, high resolution (e.g. at least annual) paleoclimate proxy records, particularly in the densely populated eastern seaboard. Of the existing eastern Australian-based streamflow reconstructions (Table 1), two (from the island of Tasmania) utilise local proxy (tree ring) records (4 and 5, Fig. 1a) (Allen et al., 2015a; Allen et al., 2015b; Allen et al., 2017). The remaining reconstructions use proxy records that are remote from the water catchments of interest and therefore rely on climatic teleconnections between the proxy location and the region of interest. McGowan et al. (2009) produced a streamflow reconstruction for the River Murray (2, Fig. 1a) based on a reconstruction of the Pacific Decadal Oscillation (PDO) which in turn was developed from flood-drought records in eastern China. Gallant and Gergis (2011) produced a streamflow reconstruction for the same location as McGowan et al. (2009) (3, Fig. 1a) but used a network of tree ring and coral records from New Zealand, Indonesia, the tropical Pacific region and Australia (outside of the River Murray catchment). Finally, Lough (2007) produced streamflow reconstructions for four rivers in northeastern tropical Australia from coral records from the Great Barrier Reef (1, Fig. 1a).

A remote climate proxy record that has also been utilised for Australia is the millennial-length summer sea salt record from the Law Dome ice core in East Antarctica (Vance et al., 2013, 2015; Tozer et al., 2016). Law Dome annual sea salt concentrations are a function of wind speed over the Southern Ocean, which are connected with large-scale climate processes operating at annual to decadal scales that also influence Australia's climate (Souney et al., 2002; Vance et al., 2013, 2015). Tozer et al. (2016) recently used the sea salt proxy record to develop a 1013-year rainfall reconstruction for the Williams River (WR) catchment on the eastern seaboard of Australia (Fig. 1b). The proxy record is annually resolved and accurately dated (discussed in Section 3.1.2), enabling precise dating of extreme events. This record is also significantly longer than other proxy records (and the instrumental period) used in existing Australian streamflow reconstructions (Table 1), and has the potential for extension to 2000 years (Roberts et al., 2015). This proxy record is unique for hydroclimate studies where accurate event timing and high data resolution are needed and thus shows potential for future streamflow reconstruction in Australia.

The streamflow reconstructions presented in Table 1 are based on regression techniques. These techniques may be suitable for rainfall reconstructions, given that rainfall is directly linked with atmospheric and oceanic processes, or for tree ring based streamflow reconstructions, because tree growth is a response to local hydrologic conditions. However, for streamflow reconstructions using remote proxies, regression techniques frequently ignore other processes affecting catchment water balance (e.g. evapotranspiration, soil moisture, catchment storage, vegetation, topography, groundwater recharge) (Solander et al., 2010; Gallant and Gergis, 2011; Saito et al., 2015).

An alternative option is to develop a hydrological model that uses proxy-derived inputs to produce a streamflow reconstruction (e.g. Saito et al., 2008; Gray and McCabe, 2010; Solander et al., 2010; Saito et al., 2015). This approach incorporates catchment processes into the streamflow reconstruction development. For example, Gray and McCabe (2010) and Saito et al. (2015) reconstructed preinstrumental streamflow in two catchments in the western United States using conceptual hydrological models with tree ring-derived precipitation and temperature as inputs. However, a drawback of this approach is the need to calibrate multiple model parameters (e.g. four and six parameters in the case of Gray and McCabe (2010) and Saito et al. (2015) respectively) and the consequent assumption that optimised parameters remain valid over the reconstruction time period (i.e. over multiple centuries). A change in mean rainfall can reduce parameter transferability (Vaze et al., 2010; Coron et al., 2012), and this issue is likely to magnify when using reconstructed rainfall as a model input where multiple regime shifts occur over the last 1000 years (e.g. Tozer et al., 2016).

The zero-parameter, non-linear Budyko (1974) curve provides another option for streamflow reconstruction. Widely used in the hydrological community, the Budyko curve is a simple water balance model that describes the partitioning of rainfall into streamflow and evapotranspiration (Zhang et al., 2008; Greve et al., 2015). The Budyko curve is used to model streamflow in Australian catchments (Zhang et al., 2008; Potter and Zhang, 2009) but, to our knowledge, has not been used to reconstruct preinstrumental streamflow in eastern Australia.

In this study we use the Budyko (1974) curve and an associated single parameter Milly's β curve for comparison (Milly, 1993) (discussed further in Section 4.1), which require rainfall and potential evapotranspiration (PET) inputs, to reconstruct preinstrumental

**Table 1**
Current published eastern Australian streamflow reconstructions.

| Reference | Description | Region | Proxy used | Record availability | Reconstruction method |
|---|---|---|---|---|---|
| 1. Lough (2007) | Annual (Oct-Sep) freshwater flow into Great Barrier Reef (from reconstructions of Herbert, Burdekin, Pioneer and Fitzroy River flow) | Northeast QLD | Coral luminescence indices from corals in Great Barrier Reef region | 1631–1983 (353 years) | Linear regression |
| 2. McGowan et al. (2009) | Annual River Murray inflows | Southeast Australia | Pacific Decadal Oscillation reconstruction (developed based on flood-drought records from eastern China, (Shen et al., 2006)) | 1474–1994 (521 years) | Piecewise polynomial interpolation |
| 3. Gallant and Gergis (2011) | Annual (Aug-Jul) River Murray inflows | Southeast Australia | Tree rings (from New Zealand, Indonesia, Western Australia and Tasmania) and corals (from Fiji-Tonga, Great Barrier Reef, Indonesia) | 1783–1988 (206 years) | Principal component analysis and multiple linear regression |
| 4. Allen et al. (2015b) | Dec-Jan reconstruction of a streamflow index for central-west Tasmania and inflows to the Lake Burbury impoundment | Tasmania | Tree rings (from Tasmania) | 1530–2007 (478 years) | Nested point-by-point regression |
| 5. Allen et al. (2017) | Jul-Aug inflows to the Lake Burbury impoundment | Tasmania | Tree rings (from Tasmania) | 1731–2007 (277 years) | Principal component regression |

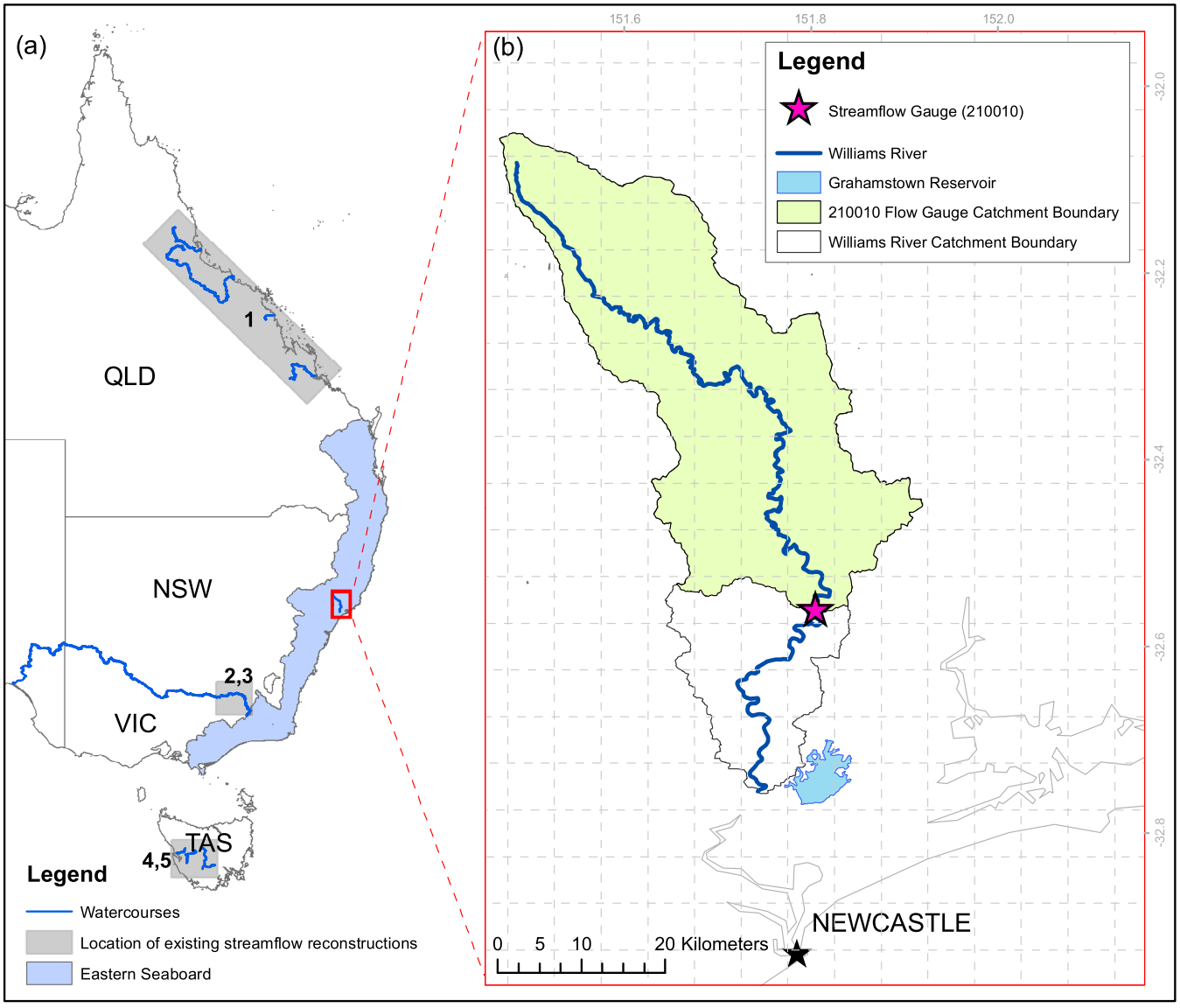


**Fig. 1.** (a) Locations of eastern Australian streamflow reconstructions: 1. Coral-based reconstruction of Lough (2007), 2. PDO-based reconstruction of McGowan et al. (2009), 3. Multi-proxy reconstruction of Gallant and Gergis (2011), 4. Tree ring-based reconstruction of Allen et al. (2015b), 5. Tree ring-based reconstruction of Allen et al. (2017). (b) WR and 210010 gauge catchment boundaries with location of streamflow gauge and Grahamstown reservoir identified.

streamflow in the WR catchment. Given that a PET reconstruction is not presently available for the WR catchment, we test two PET datasets (annual average and annually varying) over the instrumental period to determine the necessity (in terms of developing a skilful streamflow reconstruction) of reconstructing the PET variable. We also assess differences in streamflow reconstruction using two Australian gridded rainfall data products – the Scientific Information for Land Owners (SILO) database (Jeffrey et al., 2001) and Australian Water Availability Project (AWAP) (Jones et al., 2009) (Section 3.1). In addition we produce a regression based reconstruction to compare with the Budyko curve and Milly's β curve methods to identify differences in the reconstruction methods.

This study represents a novel combination of ice core science, paleoclimatology and catchment-scale hydrology. Importantly, the reconstruction provides context to the instrumental flow record and, given that a rainfall reconstruction exists for the same catchment, allows for investigation into the rainfall-runoff relationship during the instrumental and preinstrumental records. This information provides a better understanding of present infrastructure vulnerability in the context of past climate variability and allows the inference of climate variability impacts and change in water resources, climate extremes (flood, drought) and water security.

## 2. The Williams River catchment

The WR catchment is a summer/autumn rainfall dominated catchment located on the eastern seaboard of Australia (Fig. 1b). A feature of the catchment is the Grahamstown Reservoir, managed by the Hunter Water Corporation (HWC), part of the conjunctive-use headworks scheme for potable water supply in the Newcastle region (Kiem and Franks, 2004) (Fig. 1b). The Grahamstown Reservoir catchment area is too small to maintain water levels in the reservoir and hence water is extracted from WR to supplement the reservoir. Various rules exist governing how much water can be extracted from WR and includes the need to maintain environmental flows and various water constraints. One such rule is that no pumping is allowed unless streamflow volumes are above 130 ML $day^{-1}$ (Kiem and Franks, 2004). HWC use streamflow

recorded at gauge no. 210010 (Fig. 1b) to determine when and how much water should be pumped into the reservoir (Kiem and Franks, 2004), therefore we reconstructed streamflow for this gauge for the catchment specific October-September water year.

## 3. Model input data

### 3.1. Rainfall data

#### 3.1.1. Instrumental period rainfall

The WR catchment rainfall reconstruction presented in Tozer et al. (2016) was developed based on gridded rainfall from the Australian Water Availability Project (AWAP) (Jones et al., 2009). Gridded rainfall data from the Scientific Information for Land Owners (SILO) database (Jeffrey et al., 2001) is also commonly used in industry in Australia and indeed is used by HWC for input into their water resources systems. As such we use both the AWAP and SILO rainfall data in this analysis. Both AWAP and SILO products provide data resolution of 0.05° (approximately $5 \times 5$ km) and are based on interpolation of gauged rainfall data from Australia's Bureau of Meteorology. However, AWAP and SILO are produced using different interpolation techniques resulting in differences between the two products for rainfall magnitude, frequency, spatial variability, and temporal variability. See Tozer et al. (2012) for an in depth assessment of differences between, and limitations of, the AWAP and SILO rainfall products. Data is available from 1900 and 1889 to present for AWAP and SILO, respectively, however, our comparative analysis ends in September 2009. Different spatially integrated input rainfall datasets were tested within the Budyko and Milly's β curve approaches to determine both the suitability of the different models for simulating flow in the catchment and the most representative rainfall dataset to develop the 210010 catchment rainfall reconstructions. The input rainfall datasets assessed were: a '24 grid' catchment average (only grids within the catchment boundary), a '58 grid' catchment average (grids that are both within the catchment and intersect the catchment boundary), data extracted for the grid which encompasses the 210010 catchment centroid, and data from a high quality rainfall gauge (Lavery et al., 1997) within the catchment (gauge 61017). The catchment average rainfall dataset developed from the specified grids located completely within the 210010 catchment boundary (i.e. 24 grids), gave improved skill metrics (and hence improved flow simulation) relative to other input rainfall datasets. Consequently, results for the '24 grid' rainfall dataset are presented here and results using the other three input rainfall datasets are presented in the supporting information (Table S1).

#### 3.1.2. Reconstructed rainfall

Tozer et al. (2016) reconstructed a 1013-year annual rainfall record for the WR catchment from an ice core record at Law Dome, East Antarctica. Law Dome is a small independent icecap in coastal East Antarctica just south of Australia. The reconstruction exploits a relationship between sea salt concentration in snow at Law Dome and rainfall in eastern Australia identified in Vance et al. (2013) and Vance et al. (2015). The regions are linked by large-scale climate processes, in particular, the El Niño Southern Oscillation (ENSO) and associated Interdecadal Pacific Oscillation (IPO). ENSO and IPO have been identified as direct influences of climate variability across eastern Australia (e.g. McBride and Nicholls, 1983; Kiem and Franks, 2001; Kiem et al., 2003; Kiem and Franks, 2004; Risbey et al., 2009; Cai et al., 2012; Cai and van Rensch, 2013; Kiem and Verdon-Kidd, 2013) and also indirectly via their relationship with other climate processes such as the Indian Ocean Dipole (Cai et al., 2011, 2012), Southern Annular Mode (Lim et al., 2013) and blocking (i.e. mid-high latitude processes) (e.g. Pook et al., 2009).

ENSO variations extend to the mid to high latitudes and indeed there is evidence of an ENSO signature in climate records across Antarctica (Holbrook and Bindoff, 1997; Turner, 2004; Fogt and Bromwich, 2006; Clem and Fogt, 2013; Welhouse et al., 2016). At Law Dome, both ENSO and IPO signatures are identified in sea salt and snowfall accumulation rate records (Vance et al., 2013; Roberts et al., 2015; Vance et al., 2015). More specifically, sea salt variability recorded at Law Dome is related to surface wind speeds across the open ocean and is representative of large scale circulation in the mid-latitudes of the Indian and southwest Pacific Oceans (Souney et al., 2002; Goodwin et al., 2004; van Ommen and Morgan, 2010; Vance et al., 2013).

The Law Dome summer sea salt record ($LD_{SSS}$) used here was dated using annual layer counting and known volcanic age ties having an absolute accuracy from 1807 to 2009 common era (CE) and ±1 year error from 894 to 1807 CE (Plummer et al., 2012). The ±1 year error results from counting 1 year that had an ambiguous signal in some dating parameters, and the non-inclusion of another possible year that did not meet the criteria to qualify as an annual layer (year) (Curran et al., 1998; Palmer et al., 2001; Plummer et al., 2012). This highly accurate dating (over the last millennium) allows for the clear dating of extreme events that are recorded in the hydroclimate reconstructions subsequently developed from the $LD_{SSS}$ proxy record.

Tozer et al. (2016) reconstructed rainfall for each AWAP grid within the entire WR catchment (Fig. 1b) using linear regression. For this study we have developed, again using linear regression, both AWAP and SILO based reconstructions for the 210010 catchment (24 grids). A calibration period of October 1900 to September 2009 was used, based on the SILO data available for this study. The final reconstructions were scaled to have the same mean and standard deviation as the respective AWAP and SILO datasets for the 1929–2009 analysis period in order to recover variance lost during regression and allow comparison with the instrumental record (Cook et al., 2010; Allen et al., 2015b).

### 3.2. Potential evapotranspiration (PET) data

Daily PET data from the SILO database (Jeffrey et al., 2001) was used for the streamflow reconstruction as this is the dataset used by water management authorities in this region, including HWC (i.e. all hydrological/reservoir models are calibrated to SILO data meaning that, at this point in time, a reconstruction based on SILO data is more practically useful than a reconstruction based on AWAP). Tozer et al. (2012) also showed that where the spatial coverage of gauged data is reasonable (as it is in the Williams River) that the SILO product is closer to the gauged data than the AWAP product because the SILO interpolation technique involves calibrating to the gauged data whereas AWAP does not. The SILO PET dataset is developed using Morton's wet environment evapotranspiration algorithms (Vaze et al., 2010). The PET data was averaged across the 210010 gauge catchment and aggregated to an annual time step. Two variations of the PET dataset were investigated – an annually varying dataset and an annual average version calculated over the 1929–2009 period to match the availability of streamflow and rainfall data.

### 3.3. Streamflow data

All available daily streamflow data (1/12/1927-present) for gauge 210010 was obtained from the NSW Office of Water (http://realtimedata.water.nsw.gov.au/water.stm). Annual data (October to September water year) was aggregated from daily streamflow data. Nine years (1985, 1988, 1990–1992,

1996–1998, 2005) with missing daily data were removed from the October 1928 to September 2009 analysis period (end date governed by the availability of rainfall data).

Table 2 summarises the datasets used for the Budyko, Milly's β and regression models.

## 4. Annual water balance model for the Williams River catchment

### 4.1. Budyko and Budyko-like curves

Eq. (1), developed by Budyko (1974), describes the relationship between the mean annual evaporative index (ratio of catchment average actual evapotranspiration to rainfall) and dryness index (ratio of catchment average potential evapotranspiration to mean precipitation).

$$\frac{\overline{AET}}{\overline{P}} = f\left(\frac{\overline{PET}}{\overline{P}}\right) \tag{1}$$

where $\overline{AET}$ = mean actual evapotranspiration, $\overline{PET}$ = mean potential evapotranspiration, $\overline{P}$ = mean precipitation.

Assuming water storage is negligible, actual evapotranspiration (AET) is the difference between streamflow and precipitation and hence the model can be used to model mean annual streamflow (Koster and Suarez, 1999). The functional form of the Budyko curve is given in Eq. (2).

$$\frac{\overline{AET}}{\overline{P}} = \left\{\frac{\overline{PET}}{\overline{P}}\left[1 - \exp\left(-\frac{\overline{PET}}{\overline{P}}\right)\right]\tanh\left(\frac{\overline{P}}{\overline{PET}}\right)\right\}^{\frac{1}{2}} \tag{2}$$

For large values of the dryness index (PET/P), the relationship approaches the water limit (Fig. 2) where AET = precipitation (P) and for low values the relationship approaches the energy limit where AET = PET (Potter and Zhang, 2009). Values of the dryness index greater than one indicate a more arid climate and values less than one indicate a humid climate (Jones et al., 2012).

Beyond mean annual statistics, various studies have shown that the Budyko framework can be used to model interannual variability of streamflow (e.g. Koster and Suarez, 1999; Zhang et al., 2008; Potter and Zhang, 2009). In this case a key assumption is that interannual variability in surface storage is smaller than interannual rainfall, evapotranspiration and streamflow variability (Koster and Suarez, 1999). Therefore, the Budyko curve is not optimal for modelling interannual streamflow in all catchments (Potter and Zhang, 2009). Deviations from the Budyko curve occur due to local catchment conditions like soil moisture, vegetation, catchment storage and topography (e.g. Donohue et al., 2007; Zhang et al., 2008; Potter and Zhang, 2009; Jones et al., 2012; Greve et al., 2015). As such, other formulations based on the Budyko curve have been derived and include one or more free parameters designed to account for local catchment conditions (e.g. Milly, 1993; Sankarasubramanian and Vogel, 2002; Zhang et al., 2004). One such derivation is the one-parameter Milly's β curve (Milly, 1993; Potter and Zhang, 2009) given in Eq. (3). The β parameter is said to represent the reciprocal of the standardised interstorm potential evapotranspiration (Milly, 1993).

$$\frac{\overline{AET}}{\overline{P}} = \left\{exp\left[\beta\left(\frac{\overline{PET}}{\overline{P}} - 1\right)\right] - 1\right\} \Big/ \left\{exp\left[\beta\left(\frac{\overline{PET}}{\overline{P}} - 1\right)\right] - \frac{\overline{P}}{\overline{PET}}\right\} \tag{3}$$

Potter and Zhang (2009) showed that Milly's β curve with a β value of 1.98 (plotted in Fig. 2) was optimal relative to the Budyko curve and other derivations for summer rainfall dominated catchments in Australia. Fig. 2 shows the observed mean and interannual (based on SILO data) values of the evaporative and dryness indices for the 210010 catchment. Both curves provide a good match to the mean and interannual variables, however their suitability for modelling 210010 streamflow needs further investigation.

### 4.2. Testing the suitability of Budyko curves for simulating Williams River streamflow

Annual streamflow for the 210010 gauge was simulated using both Budyko's and Milly's β curves with AWAP and SILO gridded rainfall inputs (24 grids) and the PET datasets to determine which inputs provide the best streamflow simulation and ultimately whether either model could adequately simulate 210010 streamflow.

Model skill was measured via Pearson correlation (r) and associated $r^2$ metric and percent bias (difference between total simulated flow and total gauged flow as a percent of gauged). In addition we used the Nash Sutcliffe Efficiency with logarithmic values (lnNSE, Eq. (4)) and Kling-Gupta Efficiency (KGE, Eq. (5)) measures. Logarithmically transforming the streamflow values as in the lnNSE means that peak flows are flattened and low flows are given more influence (Krause et al., 2005). This is important because the magnitudes of proxy-based rainfall and streamflow reconstructions tend to have a high degree of uncertainty, particularly in extreme wet periods (e.g. Prairie et al., 2008; Tozer et al., 2016) and the traditional NSE (i.e. with untransformed flows) overemphasises large flows because any deviations are squared (Criss and Winston, 2008). The KGE is a more recently developed measure that overcomes inadequacies in the NSE. These inadequacies include using the observed mean as a baseline (Schaefli and Gupta, 2007; Gupta et al., 2009) and the fact that in order to maximise the NSE, the variability has to be underestimated (Gupta et al., 2009; Westerberg et al., 2011; Kling et al., 2012; Fowler et al., 2016). The KGE incorporates the same components of the NSE (i.e. the linear correlation (r), bias (B) and variability (γ) but separates their influence and provides a more robust indication of model skill (Gupta et al., 2009; Kling et al., 2012; Fowler et al., 2016)). We use the KGE version presented in Kling et al. (2012). Here bias is represented with B as opposed to β as it is presented in Kling et al. (2012) to avoid confusion with the Milly's β parameter.

$$lnNSE = 1 - \frac{\sum_{i=1}^{n}(lnO_i - lnS_i)^2}{\sum_{i=1}^{n}(lnO_i - lnO_i)^2} \tag{4}$$

**Table 2**
Hydrological model input data summary.

| Variable | Description | Data availability |
|---|---|---|
| Streamflow | Streamflow recorded at gauge 210010 | 1/12/1927 – present |
| PET | Annually varying PET from SILO database | 1899 – present |
| | Annual average PET from SILO database | – |
| Rainfall | AWAP rainfall averaged across grids within catchment boundary (24 grids) | 1900–2011 |
| | SILO rainfall averaged across grids within catchment boundary (24 grids) | 1900 – Aug 2010 |
| | $LD_{SSS}$ (described in Section 3.1.2) based reconstructed rainfall (calibrated to AWAP rainfall data) | 1000–2012 |
| | $LD_{SSS}$ (described in Section 3.1.2) based reconstructed rainfall (calibrated to SILO rainfall data) | 1000–2012 |

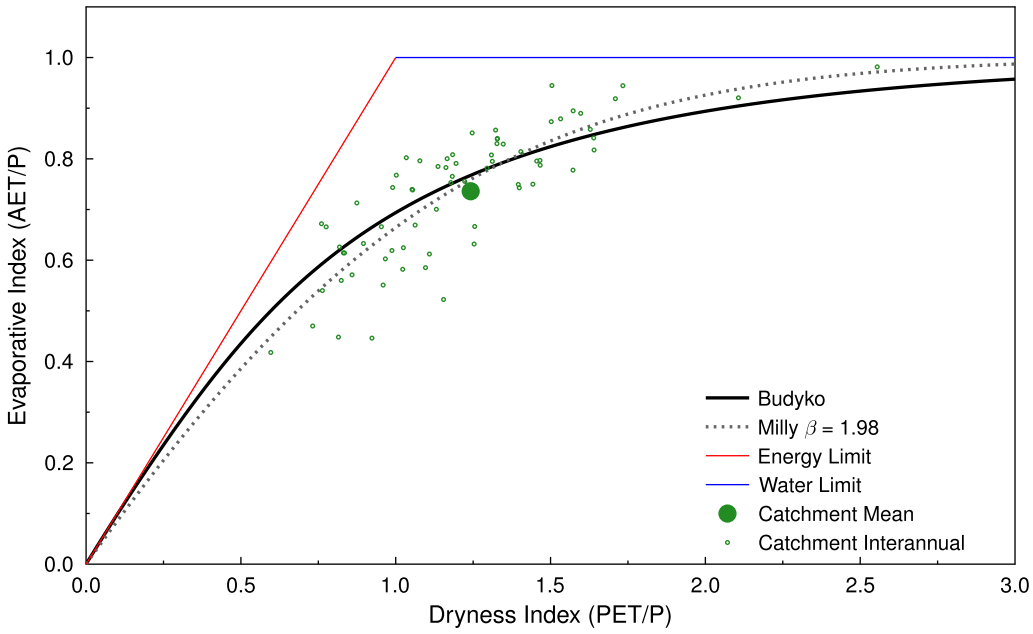


**Fig. 2.** The Budyko curve, Milly's β curves for β = 1.98, energy and water limits, mean and interannual observed data for the 210010 catchment. Catchment mean and interannual values are calculated using the SILO dataset.

where $O_i = observedflow$, $S_i = simulatedflow$.

$$KGE = 1 - \sqrt{(r-1)^2 + (B-1)^2 + (\gamma-1)^2} \quad (5)$$

where $\gamma = \frac{\sigma_s/\mu_s}{\sigma_o/\mu_o}$, $B = \frac{\mu_s}{\mu_o}$ (with μ and σ referring to mean and standard deviation respectively and subscripts o and s referring to observed and simulated flow respectively).

Skill metrics for the Budyko and Milly's β models developed with the various input datasets are presented in Table 3 with plots provided in supporting information (Figs. S1–S4). The β parameter was optimised through maximising the KGE. NSE values are also presented for comparison.

The results indicate that both the (a) Budyko and (b) Milly's β models can skilfully simulate annual streamflow at gauge 210010 with high KGE, NSE, lnNSE, r and $r^2$ values and low bias over the 1929 to 2009 analysis period. Milly's β provided slightly improved skill metrics. The optimal β values for both SILO (β = 2.14) and AWAP (β = 1.93) rainfall datasets fit well with the generic β value for summer rainfall dominated catchments identified in Potter and Zhang (2009) (β = 1.98, Section 4.1). The consistency of the calibrated β parameter over different sub-periods was also tested for the SILO dataset. The two periods (1929–1964; 1965–2009) were selected as they include 36 years of data each, noting that missing data is present in the latter half of record. Results are presented in Table 3c for SILO rainfall and SILO average PET and show similarly good performance over both sub-periods. Split sample calibration (Vaze et al., 2012) for Milly's β model was also undertaken whereby the model was calibrated to the first period and validated in the second and vice versa. Results were similar to those in Table 3 and are presented in the supporting information (Table S2). In regards to the input datasets, SILO rainfall provides slightly improved skill metrics relative to AWAP rainfall. For PET, skill metrics were similar for annually varying and annual average PET input datasets, which other authors have similarly found (Peel et al., 2000; Fowler, 2002; Oudin et al., 2005). Further discussion on the rainfall and PET input datasets is presented in Section 4.3.

### 4.3. Streamflow reconstruction

Missing data in the gauged streamflow record (see Section 3.3) was infilled using flow simulated by Milly's β model with SILO rainfall and annually varying PET inputs (calibrated to 1929–2009). This was undertaken because of the high skill of the Milly's β model in simulating 210010 streamflow (Table 3b) and so that a complete gauged streamflow record could be used for comparison with simulated flows, particularly important when investigating non-stationarity in the streamflow reconstruction skill.

The AWAP and SILO rainfall reconstructions (discussed in Section 3.1.2) were used as the rainfall input for the Budyko and Milly's β models to reconstruct streamflow for the 1929–2009 period. Results for the Budyko model are presented in Table 4a and show positive KGE values and significant correlations between gauged and reconstructed flows using all input data options. The negative lnNSE and NSE results are not desirable, however given limitations in the calculation of the NSE (discussed in Section 4.2), a negative value is not necessarily indicative of a poor model (Schaefli and Gupta, 2007; Criss and Winston, 2008), especially when magnitude is not as important as the timing and duration of wet or dry epochs, as is the case for river basins in general (e.g. van Dijk et al., 2013; Van Loon, 2015). Some variability in the strength of the relationship between the Budyko reconstructed streamflow and gauged streamflow (as measured by 10-yr moving Pearson correlation) is evident (Fig. 3). This is likely governed by non-stationarity in the relationship between $LD_{SSS}$ and rainfall in eastern Australia, which Vance et al. (2013) and Vance et al. (2015) suggest is related to the IPO, whereby the link between the regions is strengthened in IPO positive phase due to a more meridional atmospheric pressure pattern relative to the IPO negative phase. Reconstruction skill over IPO phases for the Budyko model was assessed (Table 4b) and it is indeed evident that there is reduced skill in the negative IPO phase and an increase in skill in the second positive IPO phase and combined positive phases. Tozer et al. (2016) noted, however, that this relationship is further complicated in the WR catchment due to the influence of East Coast Lows (ECL), intense storms that contribute around 25% of the region's annual rainfall. These storms are thought to contribute

**Table 3**
Skill metrics for gauged flow compared with flows simulated using (a) the Budyko model and (b) Milly's β model for different gridded input rainfall and PET datasets the 1929–2009 period. For (c) the calibrated β parameter from (b) was tested over different sub-periods (1929–1964, 1965–2009). Confidence intervals were developed using Fisher's r-to-z transformation (Fisher, 1915, 1921). Where the confidence interval does not cross 0, the result is significant. The KGE, NSE and lnNSE range from $-\infty$ to 1.

| PET | Rainfall | β | KGE | r (95% conf. int.) | $r^2$ | NSE | lnNSE | BIAS (%) |
|---|---|---|---|---|---|---|---|---|
| *(a) BUDYKO* | | | | | | | | |
| SILO varying | SILO | N/A | 0.81 | 0.93 (0.89;0.95) | 0.86 | 0.83 | 0.84 | −5.5 |
| | AWAP | N/A | 0.78 | 0.92 (0.87;0.95) | 0.84 | 0.77 | 0.81 | −12.5 |
| SILO average | SILO | N/A | 0.77 | 0.94 (0.90;0.96) | 0.88 | 0.83 | 0.83 | −6.9 |
| | AWAP | N/A | 0.74 | 0.92 (0.88;0.95) | 0.85 | 0.75 | 0.79 | −13.7 |
| *(b) Milly's β (calibrated to 1929–2009 period)* | | | | | | | | |
| SILO Varying | SILO | 2.12 | 0.90 | 0.93 (0.88;0.95) | 0.86 | 0.85 | 0.90 | −4.4 |
| | AWAP | 1.93 | 0.86 | 0.92 (0.87;0.95) | 0.84 | 0.83 | 0.85 | −5.9 |
| SILO Average | SILO | 2.14 | 0.87 | 0.94 (0.90;0.96) | 0.88 | 0.86 | 0.91 | −6.6 |
| | AWAP | 1.94 | 0.83 | 0.92 (0.88;0.95) | 0.85 | 0.82 | 0.85 | −7.7 |
| *(c) Milly's β (calibrated to 1929–2009, tested on 1929–1964 and 1965–2009 sub-periods)* | | | | | | | | |
| SILO Average | SILO (1929–1964) | 2.14 | 0.87 | 0.93 (0.86;0.96) | 0.86 | 0.83 | 0.83 | −10.7 |
| | SILO (1965–2009) | 2.14 | 0.84 | 0.95 (0.90;0.97) | 0.90 | 0.89 | 0.94 | −1.4 |

**Table 4**
Skill metrics for annual gauged flow compared with flows simulated using (a) the Budyko model (b) Budyko model for IPO phases with SILO average PET and SILO rainfall (c) Milly's β model for the 1929–2009 period using reconstructed rainfall inputs (d) Milly's β model calibrated to IPO negative (1947–1975), (e) Milly's β model calibrated to IPO positive phases (1929–1941, 1979–1997), (e) linear regression and Confidence intervals were developed using Fisher's r-to-z transformation (Fisher, 1915, 1921). Where the confidence interval does not cross 0, the result is significant. The KGE, NSE and lnNSE range from $-\infty$ to 1. Note that in the IPO analyses, due to data availability, the first IPO positive phase commences in 1929 as opposed to the commonly acknowledged 1924 (Power et al., 1999).

| PET | Gridded rainfall dataset used for rainfall reconstruction | β | KGE | r (95% conf. int.) | $r^2$ | NSE | lnNSE | BIAS (%) |
|---|---|---|---|---|---|---|---|---|
| | | | *(a) BUDYKO* | | | | | |
| SILO varying | SILO | N/A | 0.31 | 0.35 (0.14;0.53) | 0.12 | −0.06 | −0.02 | −13.6 |
| | AWAP | N/A | 0.30 | 0.35 (0.14;0.53) | 0.12 | −0.06 | −0.03 | −18.8 |
| SILO average | SILO | N/A | 0.27 | 0.31 (0.10;0.50) | 0.10 | −0.10 | −0.05 | −14.3 |
| | AWAP | N/A | 0.26 | 0.31 (0.10;0.50) | 0.10 | −0.10 | −0.06 | −19.5 |
| | | | *(b) BUDYKO – IPO Phases* | | | | | |
| SILO average | SILO | N/A | | | | | | |
| | Positive (1929–1941) | | 0.22 | 0.23 (−0.37; 0.69) | 0.05 | −0.44 | −0.20 | −13.3 |
| | Positive (1979–1997) | | 0.57 | 0.59 (0.19; 0.83) | 0.35 | −0.04 | 0.26 | 9.3 |
| | Combined Positive | | 0.44 | 0.45 (0.12; 0.69) | 0.20 | −0.18 | 0.20 | −1.2 |
| | Negative (1947–1975) | | 0.22 | 0.38 (0.02; 0.66) | 0.15 | 0.02 | 0.08 | −24.9 |
| | | | *(c) Milly's β (calibrated to 1929–2009 period and reconstructed rainfall)* | | | | | |
| SILO Varying | SILO | 1.90 | 0.34 | 0.35 (0.14; 0.53) | 0.12 | −0.14 | −0.19 | −5.8 |
| SILO Average | SILO | 1.88 | 0.30 | 0.31 (0.10; 0.50) | 0.10 | −0.18 | −0.20 | −5.7 |
| | | | *(d) Milly's β (calibrated to IPO negative phase, validated on remaining data)* | | | | | |
| SILO average | SILO (1947–1975) | 1.86 | 0.28 | 0.29 (0.02; 0.52) | 0.09 | −0.71 | −0.39 | 3.3 |
| | SILO (1929–1946, 1976–2009) | 1.86 | 0.26 | 0.38 (0.02; 0.66) | 0.15 | 0.07 | 0.03 | −16.2 |
| | | | *(e) Milly's β (calibrated to IPO positive phases, validated on remaining data)* | | | | | |
| SILO average | SILO (1929–1941, 1979–1997) | 1.80 | 0.42 | 0.45 (0.12; 0.69) | 0.20 | −0.51 | 0.12 | 11.1 |
| | SILO (1942–1978, 1998–2009) | 1.80 | 0.19 | 0.23 (−0.05; 0.48) | 0.05 | −0.17 | −0.51 | −9.2 |
| | | | *(f) Linear regression* | | | | | |
| N/A | N/A | N/A | 0.31 | 0.31 (0.10; 0.50) | 0.10 | −0.37 | N/A | 0.0 |

to the nonstationarity in the relationship between $LD_{SSS}$ and climate variability in the WR catchment and may also explain the reduced skill in the first positive IPO phase (i.e. the clear IPO-related variability in the $LD_{SSS}$-rainfall link identified in Vance et al. (2013) and Vance et al. (2015) for southeast QLD does not always hold for the WR catchment (Tozer et al., 2016)). This may also be compounded by the relatively short analysis period available for the first positive IPO phase (13 years compared with 19+ years for other periods) or issues with the gauged flow early in the record. Of importance is that while there is acknowledged non-stationarity in the link between Law Dome and the WR catchment, the annual correlation remains greater than 0.23 during all phases.

The Milly's β model was initially run with parameter values from the gauged data analysis (Table 3), however improvement in skill was found with calibrating directly to the reconstructions (Table 4c). Results using β values from the gauged data analysis are presented in Table S3 in the supporting information. The KGE was again used as the objective function. Also shown are the results for a linear least squares regression model. The regression based reconstruction was scaled to have the same mean and standard deviation as the streamflow data over the 1929–2009 analysis period, hence the bias is 0% (Table 4f).

For the two input rainfall reconstructions (Table 4a), the SILO based reconstruction provided marginally improved statistics relative to the AWAP based reconstruction. The correlation values (r) and consequently $r^2$ determined for both reconstructions are very similar because the rainfall reconstructions account for the same amount of variability in the respective gridded rainfall they were developed from (11.5% and 11.8% of the annual AWAP and SILO gridded datasets). These results show that the accuracy of the 210010 streamflow reconstruction is not that sensitive to the gridded rainfall data product used.

A 2% increase in the gauged streamflow variability accounted for, is observed for the models using the annually varying PET compared with average PET (Table 4a for Budyko and Table 4c for Milly's β results). Annual rainfall variability is the primary driver

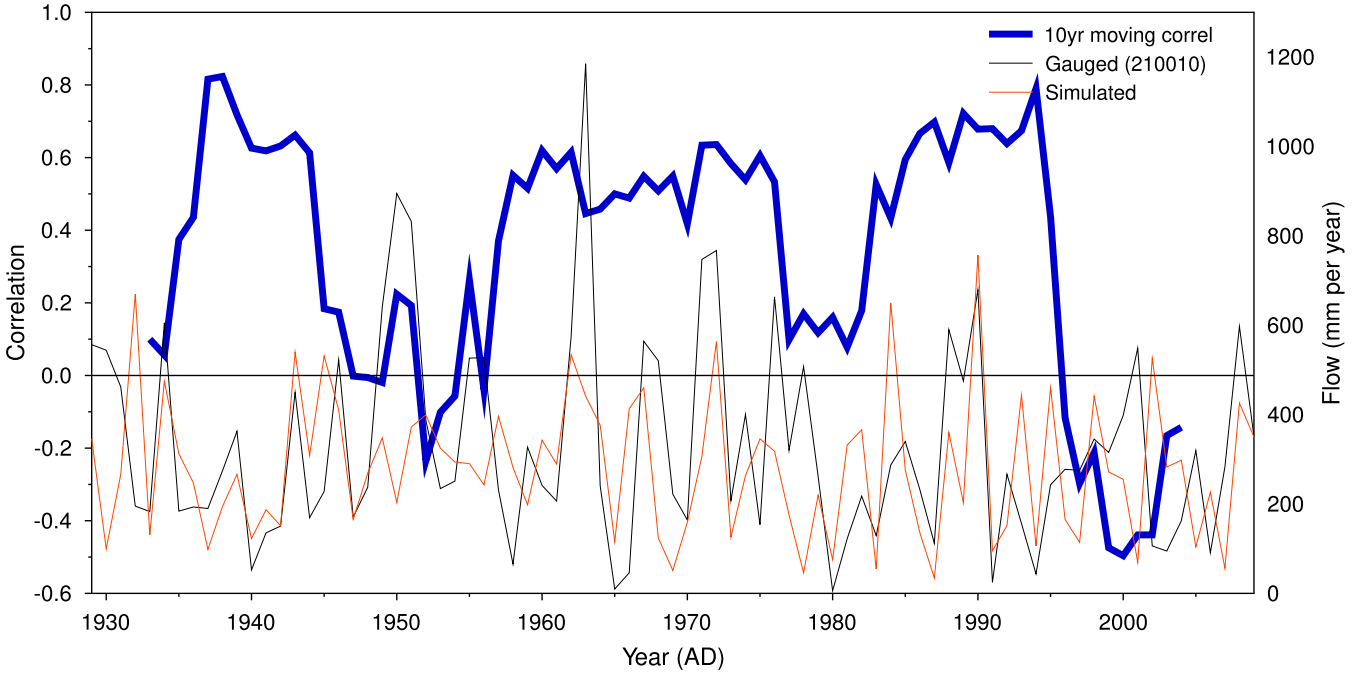


**Fig. 3.** 10-yr running correlation between gauged (210010) streamflow and streamflow reconstructed using the Budyko model with SILO reconstructed rainfall and SILO average PET. Also included are the timeseries of gauged and simulated annual flows (October-September water year).

of annual streamflow variability (Koster and Suarez, 1999; Arora, 2002; Potter and Zhang, 2009), likely due to its high interannual variability relative to PET (annual rainfall variability is typically 20–25% compared with ~5% for PET) (Peel et al., 2000). Nonetheless, PET and local catchment characteristics like antecedent soil moisture storage conditions are important components of the water balance (Wooldridge et al., 2001) and although based on these results one could conclude that average PET is adequate for modelling preinstrumental streamflow, it is not clear whether the ~5% interannual variability seen in the gauged PET record was greater in the past. If interannual variability in PET was greater (or different) in the past this may change the influence of PET on the water balance and warrant the development of a PET reconstruction. However, a PET reconstruction would bring with it the typical uncertainties associated with the reconstruction process (e.g. non-stationarity in the relationship between the proxy and gauged climate variable (Gallant et al., 2013; Batehup et al., 2015)) and again it is unclear whether these uncertainties would be lower than uncertainties associated with using annual average values from the instrumental period and applying it back in time. As such, for the purposes of the study, we use average PET to develop our streamflow reconstruction (Section 5).

Comparing the two models, the Milly's β models (Table 4c) provided improved KGE and bias statistics relative to the Budyko models (Table 4a) but poorer NSE and lnNSE results. This is not unexpected given that the Milly's β models were optimised relative to the KGE and not the NSE and lnNSE. Clearer improvement in the streamflow reconstructions produced using Milly's β model relative to Budyko is seen in Fig. 4a and b (for SILO rainfall) where a closer match to gauged flows is evident, particularly for high flow periods. Though it has only one parameter, a potential limitation of using Milly's β for reconstructing climate is the assumption of parameter stability over time. As discussed in Section 1, model parameters are sensitive to the climate during the calibration period (Saft et al., 2016) which might affect their transferability outside of this period (Vaze et al., 2010; Coron et al., 2012). Kiem and Franks (2004) showed for the WR catchment that rainfall and streamflow in IPO positive and negative phases are significantly different whereby higher (lower) and more (less) variable rainfall/streamflow is recorded in IPO negative (positive) phase. We confirmed these results using the annual 210010 streamflow and SILO 24 grid average rainfall and results are presented in Figs. S7 and S8 and Table S4 in the supporting information. Given the different climate regimes in the IPO phases, we tested the transferability of the Milly's β parameter by calibrating first to the IPO negative phase (1947–1975) and validating on the remaining data and then calibrating to IPO positive phases (1929–1941, 1979–1997) and validating on the remaining data. Results are presented in Table 4d and e. Firstly, there is little variation in parameter values across the three calibration periods tested (1929–2009, IPO negative, IPO positive). Skill metrics for the calibration to IPO negative (Table 4d) and validating to the remainder of the data were generally reduced for the calibration period compared to validation, particularly the NSE and lnNSE. This is not surprising given: the use of KGE as the objective function (as opposed to optimising the NSE or lnNSE); that the NSE is known to emphasise large flows (Section 4.2) and IPO negative is a particularly wet period; and there is a reduced connection between Law Dome and eastern Australia in IPO negative (Vance et al., 2015). Results for calibrating to IPO positive (Table 4e) show improved metrics for the calibration period, as one would expect, relative to validation. This suggests some issues with parameter transferability however this relates less to Milly's β model and more to the variability in the strength of the relationship between $LD_{SSS}$ and rainfall (further discussed in Tozer et al. (2016)). Non-stationarities in the proxy and gauged climate relationship is a concern for all proxy based climate reconstructions, as mentioned above (Gallant et al., 2013; Batehup et al., 2015).

The regression, Budyko and Milly's β model based reconstructions are similar (Fig. 4a and b) and have comparable skill metrics which again suggests that rainfall variability is the key driver of streamflow variability at this timeframe. However, the regression method provides a physically unrealistic streamflow reconstruction (i.e. negative flows) and this emphasises the importance of

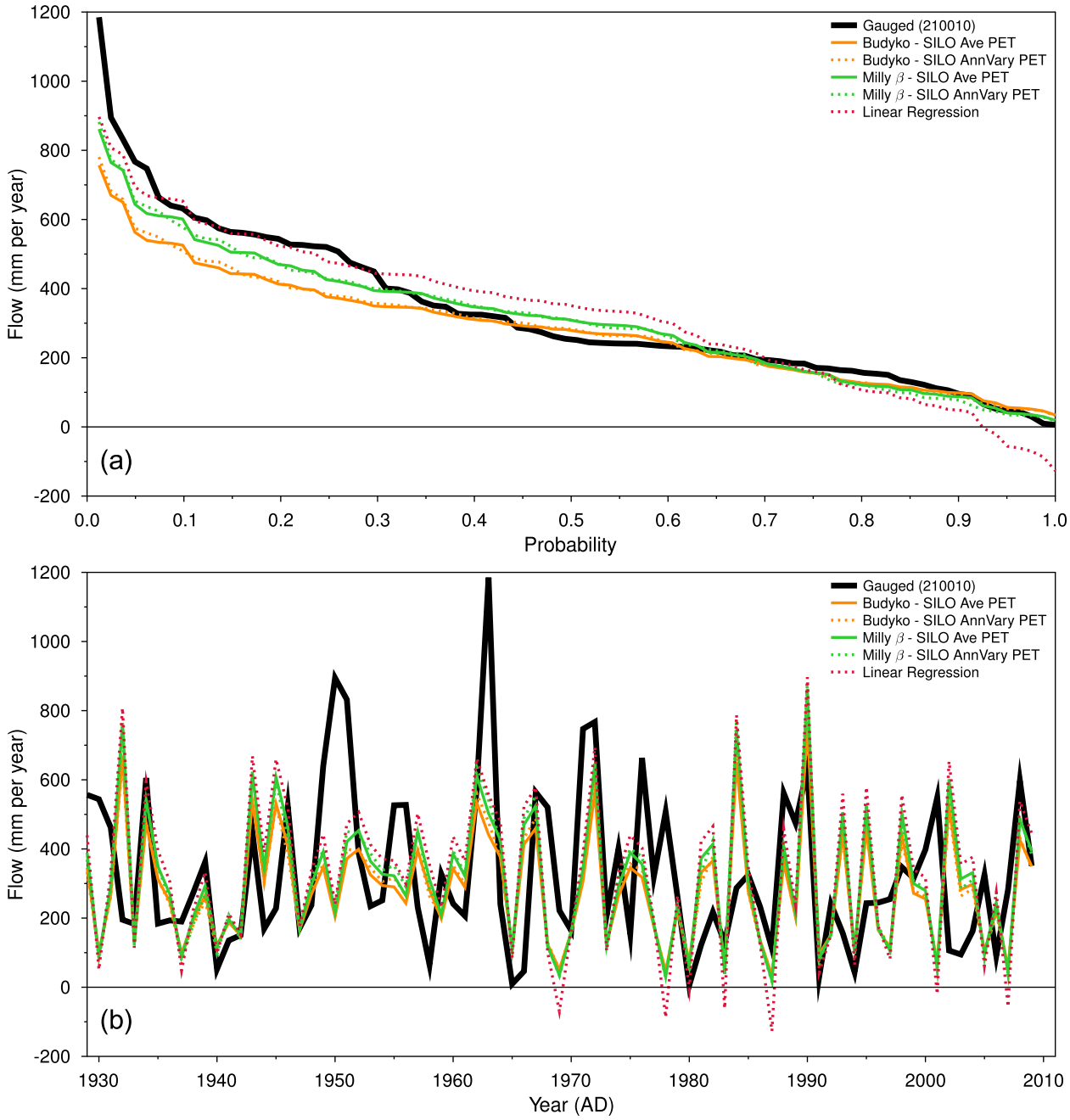


**Fig. 4.** (a) Flow duration curve and (b) Timeseries comparison of gauged flow and reconstructed flow based on linear regression and flow simulated using the Budyko and Milly's β models with SILO based rainfall reconstruction and SILO annually varying (SILO AnnVary PET) and average PET (SILO Ave PET). Plots for AWAP rainfall datasets are provided in the supporting information.

using a method for reconstructing streamflow that is both physically realistic (i.e. able to account for non-linearities inherent in converting rainfall to runoff) and satisfactory in terms of performance statistics. A comparison of reconstructions produced using AWAP rainfall are presented in Figs. S5 and S6 in the supporting information.

The results presented in Section 4.3 show that:

- A skilful streamflow reconstruction can be developed for the 210010 gauge using both Budyko & Milly's β models with reconstructed rainfall derived from the $LD_{SSS}$ proxy.
- Both AWAP and SILO rainfall products are suitable as model inputs.
- Annually varying PET provides a slight increase in skill but reconstruction of this variable is associated with additional uncertainties which need to be weighed relative to the potential increase in reconstruction skill.
- The hydrological modelling approach provides for a more physically realistic streamflow reconstruction relative to the linear regression approach.

Reconstruction skill may be further improved with the addition of other proxies including those from the Law Dome ice core (Roberts et al., 2015); new ice core records from other East Antarctica sites (Vance et al., 2016); and from other proxies within or near Australia that are influenced by similar climate processes

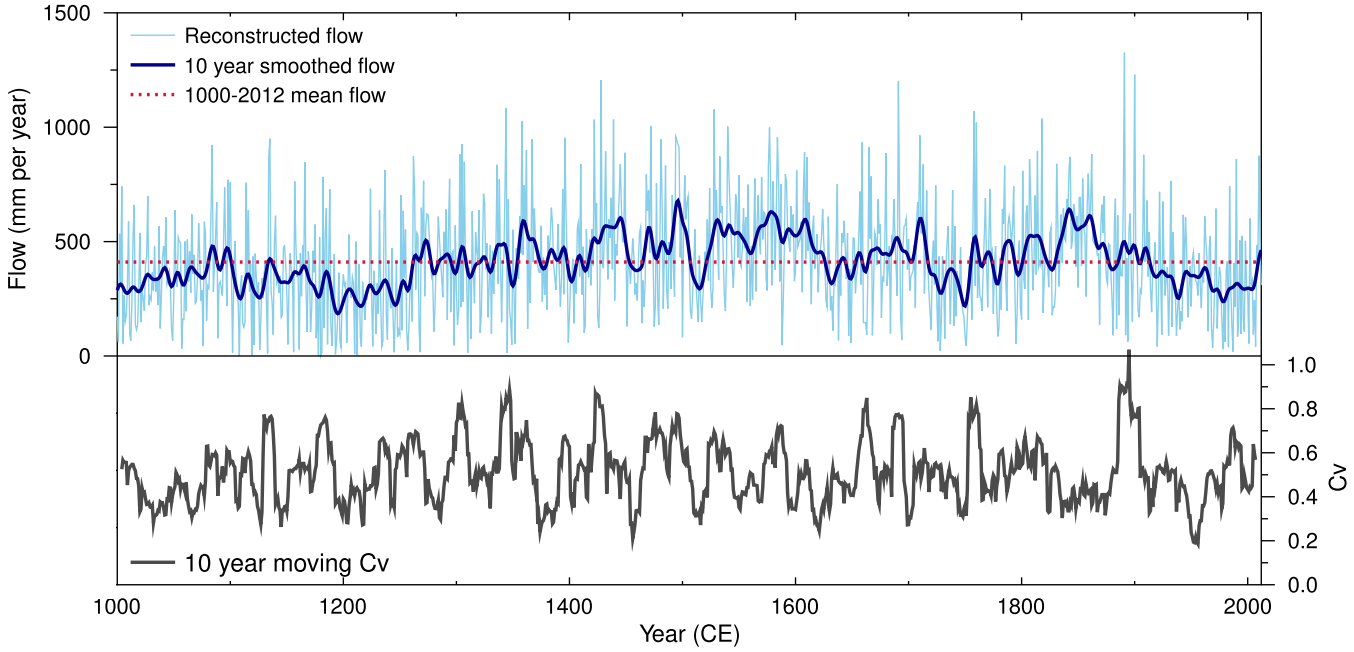


**Fig. 5.** Annual streamflow reconstruction (thin light blue line), 10 year Gaussian smoothed streamflow reconstruction (thick dark blue line) and mean reconstruction flow (dotted red line) produced using Milly's β model with SILO based rainfall reconstruction and SILO average PET. 10 year moving coefficient of variation (Cv) also shown (thick grey line) in the bottom panel. (For interpretation of the references to colour in this figure legend, the reader is referred to the web version of this article.)

(e.g. Gallant and Gergis, 2011; Palmer et al., 2015). These are avenues for future research but it should also be acknowledged that inclusion of additional proxy information may not always improve reconstruction skill and can potentially introduce extra uncertainties to the reconstruction process due to inconsistencies in the climate signals represented in the individual proxies (e.g. Wilson et al., 2010; Vance et al., 2017).

## 5. Millennial length streamflow reconstruction

Based on the above findings, a 1013-year (1000–2012 CE) streamflow reconstruction was developed for the 210010 gauge using Milly's β model (with $\beta = 1.88$) with the SILO based rainfall reconstruction and SILO average PET inputs. The reconstruction (annual and 10-year smoothed) is presented in Fig. 5 along with a timeseries of the 10 year running coefficient of variation (Cv), calculated as the ratio of the running standard deviation to the long-term mean for the 1929–2009 period. As streamflow variability increases (i.e. Cv approaches 1) so too does the vulnerability of infrastructure (McMahon et al., 2006), hence the ability to put instrumental period streamflow variability into a long-term context is important.

Fig. 5 indicates several periods in the preinstrumental period that are characterised by high variability relative to the instrumental record, particularly the late 1800s and 1300–1500s. Importantly, Fig. 5 shows that 210010 streamflow oscillates between periods of low and high variability suggesting that infrastructure vulnerability similarly oscillates over time. This indeed highlights the decadal to centennial scale cycles inherent in our climate (e.g. Power et al., 1999; Gallant et al., 2013) and the need to look beyond our short instrumental period to fully understand current climate risks.

The reconstruction (Fig. 5) shows long (decadal and longer) periods of above and below mean streamflow. The duration of these periods are important in water resource management. Wet and dry epochs in the rainfall and streamflow reconstructions were determined based on Eq. (6), following Tozer et al. (2016).

$$\begin{aligned} wet = {} & years\ where\ reconstruction \\ & > mean - 0.3 \times standard\ deviation dry \\ = {} & years\ where\ reconstruction \\ & < mean + 0.3 \times standard\ deviation \end{aligned} \quad (6)$$

This threshold is designed to identify periods that are generally wet or generally dry even though some years within that period are slightly below or above the long-term average (e.g. one high streamflow year within a particularly dry period may not fill a reservoir). The same wet/dry epoch definition is used for rainfall and streamflow despite these variables having different annual distributions both in general and as also evident in the two reconstructions (see Fig. S9 in supporting information). The use of the same procedure allows us to assess the variability of wet/dry epoch duration between the two variables, which is important for determining lags in streamflow recovery and meteorological drought, for example (Yang et al., 2017).

Table 5 identifies wet and dry epochs of at least 5 years duration in the (a) gauged streamflow data (b) reconstructed streamflow data over the 1929–2009 period and (c) reconstructed streamflow over the full 1000–2012 year period. Firstly the wet and dry epochs identified in the reconstructed data (Table 5b) are compared with those identified in the gauged data (Table 5a) over the instrumental period. Importantly, the rainfall and streamflow reconstructions both capture the major World War II (1935–1942) and Millennium (2002–2007) droughts (Verdon-Kidd and Kiem, 2009). Some dry events identified in the gauged records are not captured in the reconstructions, however there is some ambiguity in the 1991–2000 dry event whereby the gauged record provided partially falls within the wet epoch list. The wet epochs are reasonably captured in both the rainfall and streamflow reconstructions acknowledging that the $LD_{SSS}$ proxy is least accurate in extreme wet epochs (Tozer et al., 2016), which no annually resolved proxy is likely to capture. Thus, the rainfall and streamflow reconstructions adequately capture the duration of gauged wet and dry epochs, which provides further validation (beyond

**Table 5**
Identification of wet and dry epochs of at least 5 years in length in rainfall and streamflow records for (a) gauged/gridded data over the instrumental period (b) reconstructed data over the instrumental period (c) reconstructed data over the full reconstruction period. Epochs defined using Eq. (6) with mean and standard deviation calculated over the 1929–2009 period. Epochs are listed in chronological order. Only wet epochs ≥ 10 years are shown in (c).

| Climate variable | Relevant statistics (1929–2009) | Dry epoch (No. of years) | Wet epoch (No. of years) |
|---|---|---|---|
| *(a) GAUGED DATA (1929–2009)* | | | |
| Rain (based on SILO catchment average) | Mean = 1133.5 Std. Dev. = 281.3 | 1935–1942 (8)<br>1979–1983 (5)<br>1991–2000 (10)<br>2002–2007 (6) | 1948–1956 (9)<br>1959–1963 (5)<br>1995–2001 (7) |
| Streamflow (Gauge 210010) | Mean = 329.9 Std. Dev. = 225.8 | 1935–1942 (8)<br>1957–1961 (5)<br>1979–1987 (9)<br>1991–1999 (9)<br>2002–2007 (6) | N/A |
| *(b) RECONSTRUCTED DATA (1929–2009)* | | | |
| Reconstructed Rain (based on SILO catchment average) | Mean = 1086.1 Std. Dev. = 279.4 | 1935–1942 (8)<br>2003–2007 (5) | 1951–1958 (8)<br>1960–1964 (5) |
| Reconstructed Streamflow (based on Milly's β) | Mean = 311.2 Std. Dev. = 188.7 | 1935–1942 (8)<br>1976–1980 (5)<br>2003–2007 (5) | 1951–1958 (8)<br>1960–1964 (5) |
| *(c) RECONSTRUCTED DATA (1000–2012)* | | | |
| Reconstructed Rain (based on SILO catchment average) | Mean = 1086.1 Std. Dev. = 279.4 | 1005–1009, 1089–1093 (5)<br>1123–1129 (7)<br>1141–1146 (6)<br>1206–1210 (5)<br>1215–1223 (9)<br>1256–1261 (6)<br>1631–1635 (5)<br>1747–1753 (7)<br>1935–1942 (8)<br>2003–2007 (5) | 1269–1279 (11)<br>1282–1291 (10)<br>1353–1362 (10)<br>1366–1379 (14)<br>1381–1391 (11)<br>1415–1424 (10)<br>1427–1450 (24)<br>1452–1463 (12)<br>1488–1499 (12)<br>1527–1537 (11)<br>1539–1559 (21)<br>1561–1587 (27)<br>1590–1613 (24)<br>1615–1627 (13)<br>1650–1659 (10)<br>1695–1705 (11)<br>1707–1718 (12)<br>1807–1818 (12)<br>1830–1868 (39)<br>1870–1880 (11)<br>1905–1914 (10) |
| Reconstructed Streamflow (based on Milly's β) | Mean = 311.2 Std. Dev. = 188.7 | 1005–1009, 1028–1032,<br>1089–1093 (5)<br>1105–1113 (9)<br>1123–1130 (8)<br>1141–1146 (6)<br>1193–1204 (12)<br>1206–1210 (5)<br>1215–1223 (9)<br>1256–1261 (6)<br>1631–1635, 1660–1664 (5)<br>1747–1753 (7)<br>1935–1942 (8)<br>1976–1980, 2003–2007 (5) | 1269–1279 (11)<br>1282–1291 (10)<br>1353–1362 (10)<br>1366–1375 (10)<br>1381–1391 (11)<br>1415–1424 (10)<br>1427–1439 (13)<br>1441–1450 (10)<br>1488–1499 (12)<br>1527–1537 (11)<br>1539–1556 (18)<br>1563–1587 (25)<br>1590–1613 (24)<br>1615–1626 (12)<br>1650–1659 (10)<br>1695–1705 (11)<br>1707–1718 (12)<br>1807–1818 (12)<br>1830–1868 (39)<br>1870–1879 (10)<br>1905–1914 (10) |

the skill metrics presented in Table 4) for the use of the $LD_{SSS}$ proxy in reconstructing eastern Australian hydroclimate.

Next, the differences in epoch lengths in the streamflow and rainfall records are assessed to gain further insights into the rainfall-runoff relationship during preinstrumental and instrumental periods. In comparing the gauged streamflow record with gauged rainfall record (Table 5a), it is apparent that differences exists between the number and length of epochs identified. For example an additional dry epoch is identified in the gauged streamflow record (1957–1961) and a corresponding dry rainfall epoch is longer in the streamflow record (i.e. 1979–1983 in the rainfall record compared with 1979–1987 in the streamflow record). In the wet epochs there were no wet streamflow epochs that met the criteria of at least 5 years in length. These results indi-

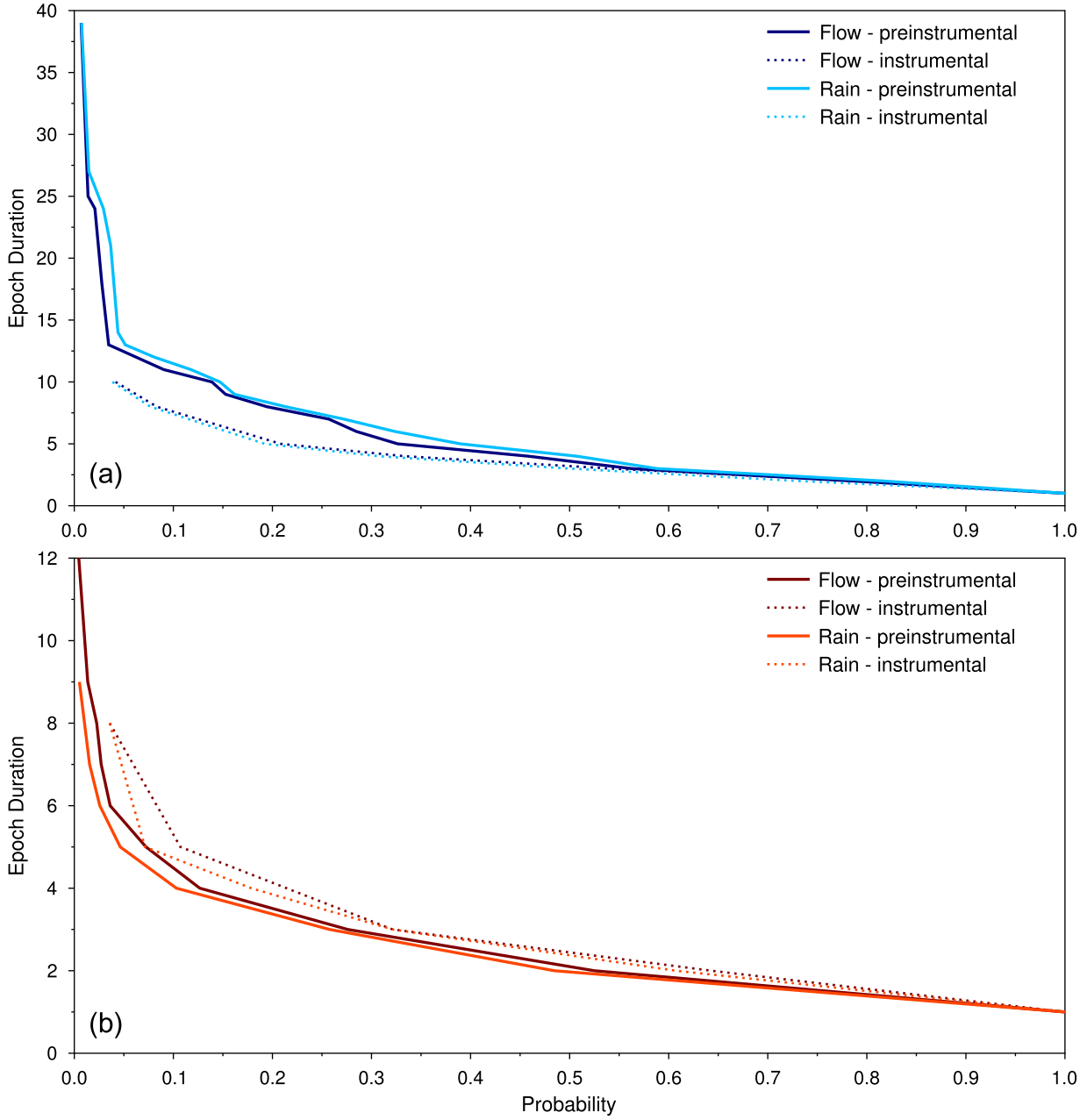


**Fig. 6.** Probability curves of (a) wet epoch duration and (b) dry epoch duration for 210010 streamflow and catchment rainfall for preinstrumental (pre-1900) and instrumental period.

cate that dry (wet) periods are longer (shorter) in the gauged rainfall than in the gauged streamflow record. For the reconstructed data over the gauged period (Table 5b) there are additional dry epochs in the streamflow record that are not present in the rainfall record, though no differences are seen in wet epochs that are identified in the reconstructed rainfall and streamflow over the instrumental period. Assessing the reconstruction over the full 1000–2012 period (Table 5c) further supports the trend identified above. That is, more dry epochs are present in the streamflow record relative to rainfall record (11 epochs of at least 5 years in the rainfall record and 16 in the streamflow record). In addition, longer epochs are present in the streamflow record relative to rainfall (e.g. the longest epoch in streamflow record is 12 years (1193–1204) compared with 9 years in the rainfall record (1215–1223) and the 1193–1204 dry streamflow period is not identified as a dry epoch in the rainfall record. Given the large number of wet epochs of 5 years and greater identified, only those greater than 10 years are presented in Table 5c (all epochs are provided in Table S5 in the supporting information). There are 58 5-year wet epochs identified in the rainfall record relative to 52 in the streamflow record (supporting information). Furthermore, several wet epochs are shorter in the streamflow record relative to the rainfall record. For example, the wet epoch commencing in 1539 is 21 years long in the rainfall record but only 18 years in the streamflow record and similarly the epoch commencing in 1452 is 12 years long in the rainfall record but not present in the reconstructed streamflow record (Table 5c) because it is only 8 years long. These results suggest that a long wet/dry rainfall period will not necessarily translate to the same length wet/dry period in streamflow. Despite rainfall variability being the primary driver of streamflow variability at the

annual scale (discussed in Section 4.2), non-linearity in the rainfall-streamflow relationship is also influenced by PET and local catchment characteristics like antecedent soil moisture conditions, as mentioned, (e.g. Wooldridge et al., 2001; Saft et al., 2015; Yang et al., 2017), and this has implications for interpreting rainfall proxies as indicators of water availability or water security. These findings also highlight the importance of distinguishing between extreme rainfall and flooding (e.g. Johnson et al., 2016) and the different types of drought (e.g. meteorological, hydrological, agricultural droughts) (e.g. Kiem et al., 2016) when assessing impacts and looking to manage current and future hydroclimatic risks.

The results in Table 5 also indicate that different centuries are dominated by different climate regimes and that the frequency of these epochs varies from century to century. For example, the 1100s to mid-1200s was a predominantly dry epoch along with the post-1900s period. Conversely, the 1300s to late 1600s and 1800s were predominantly wet epochs. This suggests that the reliance on statistics from one century (e.g. the instrumental period as is the current practice), will likely underestimate, or at least misrepresent, the true hydroclimatic risk in a given catchment or region (Tozer et al., 2016).

Epoch duration is also presented as probability of exceedance curves for wet epochs (Fig. 6a) and dry epochs (Fig. 6b). These figures both confirm the tendency for shorter (longer) duration wet (dry) epochs in the streamflow compared with the rainfall record discussed above. Importantly, these figures show that wet (dry) epoch duration in the instrumental period is markedly shorter (longer) than wet (dry) epoch duration in the preinstrumental period. For example, statistics from the instrumental record suggest that for dry epochs (Fig. 6b), there is no chance of experiencing a dry period of longer than 8 years, yet this is clearly possible when the preinstrumental record is considered. Similarly, the statistics from the instrumental period suggest that there is no chance of experiencing a wet epoch longer than 10 years but the preinstrumental streamflow record suggest a probability of at least 15% (Fig. 6a) and that wet epochs up to ~40 years duration are feasible. This is a concern given that these extended periods of wet/dry regimes are "a major cause of suboptimal operations in water supply reservoirs" (Turner and Galelli, 2016). In addition, the long duration events observed in the preinstrumental period may have implications for PET (and the meteorological variables that go into its estimation: e.g. temperature, humidity, wind speed, solar radiation) and the assumption that average PET is adequate for modelling streamflow in the preinstrumental era. Though Fowler (2002) identified comparable performance in a 13 year daily water balance model using a range of PET inputs from climatological PET to more sophisticated daily estimations and across extreme dry and wet periods, it is not certain that these results can be extrapolated to the timeframe and annual resolution investigated here. This needs further investigation but the outputs presented here (i.e. the knowledge of when and for how long wet/dry epochs occur) will be useful in undertaking investigations into long-term PET changes and their influence (or not) on streamflow variability.

## 6. Conclusions

This study presents the use of the Budyko framework to produce streamflow reconstructions as a means to overcome potential issues with regression and multi-parameter hydrological modelling approaches. The method presented and insights in regards to PET input data requirements are transferable to other catchments in Australia and elsewhere. In addition, for the first time, we have shown the utility of an ice-core based proxy in producing a skilful, millennial-length and annually resolved streamflow reconstruction in an Australian catchment.

Interrogation of the streamflow reconstruction has shown that:

- not only are longer dry/wet periods present in the preinstrumental period relative to instrumental, they are frequent;
- where there is no probability of certain duration events occurring in the instrumental record, this probability exists in the preinstrumental record;
- there have been periods of higher streamflow variability in the preinstrumental, which, if similar occurred today, relates to increased infrastructure vulnerability;
- the dominant climate regime (wet or dry) changes from century to century;
- wet (dry) epochs in the rainfall record are shorter (longer) in the streamflow record, which highlights the need for specific reconstructions of water availability instead of inferring it from rainfall proxies.

Our reliance on statistics from the instrumental period therefore means that our infrastructure design and management plans do not properly account for hydroclimatic risk in water catchments. The streamflow reconstruction better captures the range of hydroclimatic variability possible, and represents a more realistic baseline to quantify the impacts of climate variability and potential impacts of anthropogenic climate change on water security. The features identified in the reconstruction that are not evident in the instrumental period (and which we are currently not equipped to deal with) provide the first step to answering the call for incorporating streamflow reconstructions into water systems planning.

## Acknowledgements

This work was supported by the Australian Government's Cooperative Research Centres Programme through the Antarctic Climate and Ecosystems Cooperative Research Centre (ACE CRC). The Australian Antarctic Division provided funding and logistical support for the DSS ice cores (AAS projects 4061 and 4062). The Centre for Water, Climate and Land (CWCL) at the University of Newcastle provided funding for Tozer's salary. HydroTSM and HydroGOF (Zambrano Bigiarini, 2014) were used in R platform to perform some of the analysis presented here. Links to rainfall and streamflow data used in the analysis presented here are provided in Section 3. Law Dome summer sea salt data can be accessed from the Australian Antarctic Data Centre (https://data.aad.gov.au/metadata/records/summer_sea_salt_1000-2009). The authors have no conflicts of interest to declare.

## Appendix A. Supplementary data

Supplementary data associated with this article can be found, in the online version, at https://doi.org/10.1016/j.jhydrol.2018.01.064.

## References

Allen, K.J., Lee, G., Ling, F., Allie, S., Willis, M., Baker, P.J., 2015a. Palaeohydrology in climatological context: developing the case for use of remote predictors in Australian streamflow reconstructions. Appl. Geogr. 64, 132–152. https://doi.org/10.1016/j.apgeog.2015.09.007.

Allen, K.J., Nichols, S.C., Evans, R., Cook, E.R., Allie, S., Carson, G., Ling, F., Baker, P.J., 2015b. Preliminary December–January inflow and streamflow reconstructions from tree rings for western Tasmania, southeastern Australia. Water Resour. Res. 51 (7), 5487–5503. https://doi.org/10.1002/2015WR017062.

Allen, K.J., Nichols, S.C., Evans, R., Allie, S., Carson, G., Ling, F., Cook, E.R., Lee, G., Baker, P.J., 2017. A 277 year cool season dam inflow reconstruction for Tasmania, southeastern Australia. Water Resour. Res. https://doi.org/10.1002/2016WR018906.

Arora, V.K., 2002. The use of the aridity index to assess climate change effect on annual runoff. J. Hydrol. 265 (1–4), 164–177. https://doi.org/10.1016/S0022-1694(02)00101-4.

Batehup, R., McGregor, S., Gallant, A.J.E., 2015. The influence of non-stationary teleconnections on palaeoclimate reconstructions of ENSO variance using a pseudoproxy framework. Clim. Past 11 (12), 1733–1749. https://doi.org/10.5194/cp-11-1733-2015.

Biondi, F., Tomasz, J.K., Anna, K.P., 2002. Stochastic modeling of regime shifts. Clim. Res. 23 (1), 23–30 http://www.int-res.com/abstracts/cr/v23/n1/p23-30/.

Biondi, F., Kozubowski, T.J., Panorska, A.K., Saito, L., 2008. A new stochastic model of episode peak and duration for eco-hydro-climatic applications. Ecol. Model. 211 (3–4), 383–395. https://doi.org/10.1016/j.ecolmodel.2007.09.019.

Budyko, M.I., 1974. Climate and Life. Academic Press.

Cai, W., van Rensch, P., 2013. Austral summer teleconnections of Indo-Pacific variability: their nonlinearity and impacts on australian climate. J. Clim. 26 (9), 2796–2810. https://doi.org/10.1175/JCLI-D-12-00458.1.

Cai, W., Van Rensch, P., Cowan, T., Hendon, H.H., 2011. Teleconnection pathways of ENSO and the IOD and the mechanisms for impacts on Australian rainfall. J. Clim. 24 (15), 3910–3923. https://doi.org/10.1175/2011JCLI4129.1.

Cai, W., van Rensch, P., Cowan, T., Hendon, H.H., 2012. An Asymmetry in the IOD and ENSO teleconnection pathway and its impact on Australian climate. J. Clim. 25 (18), 6318–6329. https://doi.org/10.1175/JCLI-D-11-00501.1.

Clem, K.R., Fogt, R.L., 2013. Varying roles of ENSO and SAM on the Antarctic Peninsula climate in austral spring. J. Geophys. Res. Atmos. 118 (20), 11481–11492. https://doi.org/10.1002/jgrd.50860.

Cook, E.R., Meko, D.M., Stahle, D.W., Cleaveland, M.K., 1999. Drought reconstructions for the continental United States. J. Clim. 12 (4), 1145–1162. https://doi.org/10.1175/1520-0442(1999)012<1145:DRFTCU>2.0.CO;2.

Cook, E.R., Seager, R., Heim, R.R., Vose, R.S., Herweijer, C., Woodhouse, C., 2010. Megadroughts in North America: placing IPCC projections of hydroclimatic change in a long-term palaeoclimate context. J. Quat. Sci. 25 (1), 48–61. https://doi.org/10.1002/jqs.1303.

Coron, L., Andréassian, V., Perrin, C., Lerat, J., Vaze, J., Bourqui, M., Hendrickx, F., 2012. Crash testing hydrological models in contrasted climate conditions: an experiment on 216 Australian catchments. Water Resour. Res. 48 (5). https://doi.org/10.1029/2011WR011721.

Criss, R.E., Winston, W.E., 2008. Do Nash values have value? Discussion and alternate proposals. Hydrol. Process. 22 (14), 2723–2725. https://doi.org/10.1002/hyp.7072.

Curran, M.A.J., van Ommen, T.D., Morgan, V., 1998. Seasonal characteristics of the major ions in the high-accumulation Dome Summit South ice core, Law Dome, Antarctica. In: Budd, W.F. (Ed.), Annals of Glaciology. Int Glaciological Soc, Cambridge, pp. 385–390.

Donohue, R.J., Roderick, M.L., McVicar, T.R., 2007. On the importance of including vegetation dynamics in Budyko's hydrological model. Hydrol. Earth Syst. Sci. 11 (2), 983–995. https://doi.org/10.5194/hess-11-983-2007.

Elshorbagy, A., Wagener, T., Razavi, S., Sauchyn, D., 2016. Correlation and causation in tree-ring based reconstruction of paleohydrology in cold semiarid regions. Water Resour. Res.. https://doi.org/10.1002/2016WR018985.

Fisher, R.A., 1915. Frequency distribution of the values of the correlation coefficient in samples from an indefinitely large population. Biometrika 10 (4), 507–521. https://doi.org/10.2307/2331838.

Fisher, R.A., 1921. On the "probable error" of a coefficient of correlation deduced from a small sample. Metron 1, 3–32.

Fogt, R.L., Bromwich, D.H., 2006. Decadal variability of the ENSO teleconnection to the high-latitude South Pacific governed by coupling with the southern annular mode. J. Clim. 19 (6), 979–997. https://doi.org/10.1175/JCLI3671.1.

Fowler, A., 2002. Assessment of the validity of using mean potential evaporation in computations of the long-term soil water balance. J. Hydrol. 256 (3–4), 248–263. https://doi.org/10.1016/S0022-1694(01)00542-X.

Fowler, K.J.A., Peel, M.C., Western, A.W., Zhang, L., Peterson, T.J., 2016. Simulating runoff under changing climatic conditions: revisiting an apparent deficiency of conceptual rainfall-runoff models. Water Resour. Res. 52 (3), 1820–1846. https://doi.org/10.1002/2015WR018068.

Gallant, A.J.E., Gergis, J., 2011. An experimental streamflow reconstruction for the River Murray, Australia, 1783–1988. Water Resour. Res. 47 (12). https://doi.org/10.1029/2010WR009832.

Gallant, A.J.E., Phipps, S.J., Karoly, D.J., Mullan, A.B., Lorrey, A.M., 2013. Nonstationary Australasian teleconnections and implications for paleoclimate reconstructions. J. Clim. 26 (22), 8827–8849. https://doi.org/10.1175/JCLI-D-12-00338.1.

Goodwin, I.D., van Ommen, T.D., Curran, M.A.J., Mayewski, P.A., 2004. Mid latitude winter climate variability in the South Indian and southwest Pacific regions since 1300 AD. Clim. Dyn. 22 (8), 783–794. https://doi.org/10.1007/s00382-004-0403-3.

Gray, S.T., McCabe, G.J., 2010. A combined water balance and tree ring approach to understanding the potential hydrologic effects of climate change in the central Rocky Mountain region. Water Resour. Res. 46 (5). https://doi.org/10.1029/2008WR007650.

Greve, P., Gudmundsson, L., Orlowsky, B., Seneviratne, S.I., 2015. Introducing a probabilistic Budyko framework. Geophys. Res. Lett. 42 (7), 2261–2269. https://doi.org/10.1002/2015GL063449.

Gupta, H.V., Kling, H., Yilmaz, K.K., Martinez, G.F., 2009. Decomposition of the mean squared error and NSE performance criteria: implications for improving hydrological modelling. J. Hydrol. 377 (1–2), 80–91. https://doi.org/10.1016/j.jhydrol.2009.08.003.

Henley, B.J., Thyer, M.A., Kuczera, G., Franks, S.W., 2011. Climate-informed stochastic hydrological modeling: incorporating decadal-scale variability using paleo data. Water Resour. Res. 47 (11), W11509. https://doi.org/10.1029/2010WR010034.

Ho, M., Lall, U., Cook, E.R., 2016. Can a paleo-drought record be used to reconstruct streamflow? A case-study for the Missouri River Basin. Water Resour. Res. https://doi.org/10.1002/2015WR018444.

Holbrook, N.J., Bindoff, N.L., 1997. Interannual and decadal temperature variability in the Southwest Pacific Ocean between 1955 and 1988. J. Clim. 10 (5), 1035–1049. https://doi.org/10.1175/1520-0442(1997)010<1035:IADTVI>2.0.CO;2.

Jeffrey, S.J., Carter, J.O., Moodie, K.B., Beswick, A.R., 2001. Using spatial interpolation to construct a comprehensive archive of Australian climate data. Environ. Model. Softw. 16 (4), 309–330. https://doi.org/10.1016/S1364-8152(01)00008-1.

Johnson, F., White, C.J., van Dijk, A., Ekstrom, M., Evans, J.P., Jakob, D., Kiem, A.S., Leonard, M., Rouillard, A., Westra, S., 2016. Natural hazards in Australia: floods. Clim. Change 139 (1), 21–35. https://doi.org/10.1007/s10584-016-1689-y.

Jones, D.A., Wang, W., Fawcett, R., 2009. High-quality spatial climate data-sets for Australia. Aust. Meteorol. Oceanogr. J. 58, 233–248 http://www.bom.gov.au/amm/docs/2009/jones_hres.pdf.

Jones, J.A. et al., 2012. Ecosystem processes and human influences regulate streamflow response to climate change at long-term ecological research sites. Bioscience 62 (4), 390–404. https://doi.org/10.1525/bio.2012.62.4.10.

Kiem, A.S., Franks, S.W., 2001. On the identification of ENSO-induced rainfall and runoff variability: a comparison of methods and indices. Hydrol. Sci. 46 (5), 1–13.

Kiem, A.S., Franks, S.W., 2004. Multi-decadal variability of drought risk, eastern Australia. Hydrol. Process. 18 (11), 2039–2050. https://doi.org/10.1002/hyp.1460.

Kiem, A.S., Verdon-Kidd, D.C., 2013. The importance of understanding drivers of hydroclimatic variability for robust flood risk planning in the coastal zone. Aust. J. Water Resour. 17 (2), 126–134.

Kiem, A.S., Franks, S.W., Kuczera, G., 2003. Multi-decadal variability of flood risk. Geophys. Res. Lett. 30 (2), 1035. https://doi.org/10.1029/2002GL015992.

Kiem, A.S., Johnson, F., Westra, S., van Dijk, A., Evans, J.P., O'Donnell, A., Rouillard, A., Barr, C., Tyler, J., Thyer, M., Jakob, D., Woldemeskel, F., Sivakumar, B., Mehrotra, R., 2016. Natural hazards in Australia: droughts. Clim. Change 139 (1), 37–54. https://doi.org/10.1007/s10584-016-1798-7.

Kling, H., Fuchs, M., Paulin, M., 2012. Runoff conditions in the upper Danube basin under an ensemble of climate change scenarios. J. Hydrol. 424–425, 264–277. https://doi.org/10.1016/j.jhydrol.2012.01.011.

Koster, R.D., Suarez, M.J., 1999. A simple framework for examining the interannual variability of land surface moisture fluxes. J. Clim. 12 (7), 1911–1917. https://doi.org/10.1175/1520-0442(1999)012<1911:ASFFET>2.0.CO;2.

Krause, P., Boyle, D.P., Bäse, F., 2005. Comparison of different efficiency criteria for hydrological model assessment. Adv. Geosci. 5, 89–97. https://doi.org/10.5194/adgeo-5-89-2005.

Lavery, B., Joung, G., Nicholls, N., 1997. An extended high-quality historical rainfall dataset for Australia. Aust. Meteorol. Mag. 46, 27–38.

Lim, E., Hendon, H.H., Rashid, H., 2013. Seasonal predictability of the southern annular mode due to its association with ENSO. J. Clim. 26 (20), 8037–8054. https://doi.org/10.1175/jcli-d-13-00006.1.

Lough, J.M., 2007. Tropical river flow and rainfall reconstructions from coral luminescence: Great Barrier Reef, Australia. Paleoceanography 22 (2). https://doi.org/10.1029/2006PA001377.

McBride, J.L., Nicholls, N., 1983. Seasonal relationships between Australian rainfall and the southern oscillation. Mon. Weather Rev. 111 (10), 1998–2004. https://doi.org/10.1175/1520-0493(1983)111<1998:srbara>2.0.co;2.

McGowan, H.A., Marx, S.K., Denholm, J., Soderholm, J., Kamber, B.S., 2009. Reconstructing annual inflows to the headwater catchments of the Murray River, Australia, using the Pacific Decadal Oscillation. Geophys. Res. Lett. 36 (6). https://doi.org/10.1029/2008GL037049.

McMahon, T.A., Adeloye, A.J., Zhou, S.-L., 2006. Understanding performance measures of reservoirs. J. Hydrol. 324 (1–4), 359–382. https://doi.org/10.1016/j.jhydrol.2005.09.030.

Meko, D., Stockton, C.W., Boggess, W.R., 1995. The tree-ring record of severe sustained drought. J. Am. Water Resour. Assoc. 31 (5), 789–801. https://doi.org/10.1111/j.1752-1688.1995.tb03401.x.

Meko, D., Therrell, M.D., Baisan, C.H., Hughes, M.K., 2001. Sacramento river flow reconstructed to A.D. 869 from tree rings. J. Am. Water Resour. Assoc. 37 (4), 1029–1039. https://doi.org/10.1111/j.1752-1688.2001.tb05530.x.

Milly, P.C.D., 1993. An analytic solution of the stochastic storage problem applicable to soil water. Water Resour. Res. 29 (11), 3755–3758. https://doi.org/10.1029/93WR01934.

Oudin, L., Michel, C., Anctil, F., 2005. Which potential evapotranspiration input for a lumped rainfall-runoff model: Part 1 – Can rainfall-runoff models effectively handle detailed potential evapotranspiration inputs? J. Hydrol. 303 (1–4), 275–289. https://doi.org/10.1016/j.jhydrol.2004.08.025.

Palmer, A.S., van Ommen, T.D., Curran, M.A.J., Morgan, V., Souney, J.M., Mayewski, P.A., 2001. High-precision dating of volcanic events (A.D. 1301–1995) using ice cores from Law Dome, Antarctica. J. Geophys. Res. Atmos. 106 (D22), 28089–28095. https://doi.org/10.1029/2001JD000330.

Palmer, J., Cook, E.R., Turney, C.S.M., Allen, K.J., Fenwick, P., Cook, B.I., O'Donnell, A., Lough, J.M., Grierson, P., Baker, P.J., 2015. Drought variability in the eastern Australia and New Zealand summer drought atlas (ANZDA, CE 1500–2012) modulated by the Interdecadal Pacific Oscillation. Environ. Res. Lett. 10 (12), 124002 http://stacks.iop.org/1748-9326/10/i=12/a=124002.

Patskoski, J., Sankarasubramanian, A., 2015. Improved reservoir sizing utilizing observed and reconstructed streamflows within a Bayesian combination framework. Water Resour. Res. 51 (7), 5677–5697. https://doi.org/10.1002/2014WR016189.
Peel, M.C., Chiew, F.H.S., Western, A.W., McMahon, T.A., 2000. Extension of Unimpaired Monthly Streamflow Data and Regionalisation of Parameter Values to Estimate Streamflow in Ungauged Catchments. Report Prepared for the Australian National Land and Water Resources Audit, Australia, p. 37.
Plummer, C.T., Curran, M.A.J., van Ommen, T.D., Rasmussen, S.O., Moy, A.D., Vance, T.R., Clausen, H.B., Vinther, B.M., Mayewski, P.A., 2012. An independently dated 2000-yr volcanic record from Law Dome, East Antarctica, including a new perspective on the dating of the 1450s CE eruption of Kuwae, Vanuatu. Clim. Past 8 (6), 1929–1940. https://doi.org/10.5194/cp-8-1929-2012.
Pook, M.J., Lisson, S., Risbey, J., Ummenhofer, C.C., McIntosh, P., Rebbeck, M., 2009. The autumn break for cropping in southeast Australia: trends, synoptic influences and impacts on wheat yield. Int. J. Climatol. 29 (13), 2012–2026. https://doi.org/10.1002/joc.1833.
Potter, N.J., Zhang, L., 2009. Interannual variability of catchment water balance in Australia. J. Hydrol. 369 (1–2), 120–129. https://doi.org/10.1016/j.jhydrol.2009.02.005.
Power, S., Casey, T., Folland, C., Colman, A., Mehta, V., 1999. Inter-decadal modulation of the impact of ENSO on Australia. Clim. Dyn. 15 (5), 319–324. https://doi.org/10.1007/s003820050284.
Prairie, J., Nowak, K., Rajagopalan, B., Lall, U., Fulp, T., 2008. A stochastic nonparametric approach for streamflow generation combining observational and paleoreconstructed data. Water Resour. Res. 44 (6). https://doi.org/10.1029/2007WR006684.
Razavi, S., Elshorbagy, A., Wheater, H., Sauchyn, D., 2016. Time scale effect and uncertainty in reconstruction of paleo-hydrology. Hydrol. Process. 30 (13), 1985–1999. https://doi.org/10.1002/hyp.10754.
Risbey, J.S., Pook, M.J., McIntosh, P.C., Wheeler, M.C., Hendon, H.H., 2009. On the remote drivers of rainfall variability in Australia. Mon. Weather Rev. 137 (10), 3233–3253. https://doi.org/10.1175/2009MWR2861.1.
Roberts, J., Plummer, C., Vance, T.R., van Ommen, T., Moy, A., Poynter, S., Treverrow, A., Curran, M., George, S., 2015. A 2000-year annual record of snow accumulation rates for Law Dome, East Antarctica. Clim. Past 11 (5), 697–707. https://doi.org/10.5194/cp-11-697-2015.
Saft, M., Western, A.W., Zhang, L., Peel, M.C., Potter, N.J., 2015. The influence of multiyear drought on the annual rainfall-runoff relationship: an Australian perspective. Water Resour. Res. 51 (4), 2444–2463. https://doi.org/10.1002/2014WR015348.
Saft, M., Peel, M.C., Western, A.W., Perraud, J.-M., Zhang, L., 2016. Bias in streamflow projections due to climate-induced shifts in catchment response. Geophys. Res. Lett. 43 (4), 1574–1581. https://doi.org/10.1002/2015GL067326.
Saito, L., Biondi, F., Salas, J.D., Panorska, A.K., Kozubowski, T.J., 2008. A watershed modeling approach to streamflow reconstruction from tree-ring records. Environ. Res. Lett. 3 (2), 024006 http://stacks.iop.org/1748-9326/3/i=2/a=024006.
Saito, L., Biondi, F., Devkota, R., Vittori, J., Salas, J.D., 2015. A water balance approach for reconstructing streamflow using tree-ring proxy records. J. Hydrol. 529 (2), 535–547. https://doi.org/10.1016/j.jhydrol.2014.11.022.
Sankarasubramanian, A., Vogel, R.M., 2002. Annual hydroclimatology of the United States. Water Resour. Res. 38 (6), 1911–1912. https://doi.org/10.1029/2001WR000619.
Schaefli, B., Gupta, H.V., 2007. Do Nash values have value? Hydrol. Process. 21 (15), 2075–2080. https://doi.org/10.1002/hyp.6825.
Shen, C., Wang, W.-C., Gong, W., Hao, Z., 2006. A Pacific Decadal Oscillation record since 1470 AD reconstructed from proxy data of summer rainfall over eastern China. Geophys. Res. Lett. 33 (3). https://doi.org/10.1029/2005GL024804.
Solander, K., Saito, L., Biondi, F., 2010. Streamflow simulation using a water-balance model with annually-resolved inputs. J. Hydrol. 387 (1–2), 46–53. https://doi.org/10.1016/j.jhydrol.2010.03.028.
Souney, J.M., Mayewski, P.A., Goodwin, I.D., Meeker, L.D., Morgan, V., Curran, M.A.J., van Ommen, T.D., Palmer, A.S., 2002. A 700-year record of atmospheric circulation developed from the Law Dome ice core, East Antarctica ACL 1-1–ACL 1-9 J. Geophys. Res. Atmos. 107 (D22). https://doi.org/10.1029/2002JD002104.
Thyer, M., Frost, A.J., Kuczera, G., 2006. Parameter estimation and model identification for stochastic models of annual hydrological data: is the observed record long enough? J. Hydrol. 330 (1–2), 313–328. https://doi.org/10.1016/j.jhydrol.2006.03.029.
Thyer, M., Renard, B., Kavetski, D., Kuczera, G., Franks, S.W., Srikanthan, S., 2009. Critical evaluation of parameter consistency and predictive uncertainty in hydrological modeling: a case study using Bayesian total error analysis. Water Resour. Res. 45 (12). https://doi.org/10.1029/2008WR006825.
Tozer, C.R., Kiem, A.S., Verdon-Kidd, D.C., 2012. On the uncertainties associated with using gridded rainfall data as a proxy for observed. Hydrol. Earth Syst. Sci. 16 (5), 1481–1499. https://doi.org/10.5194/hess-16-1481-2012.
Tozer, C.R., Vance, T.R., Roberts, J.L., Kiem, A.S., Curran, M.A.J., Moy, A.D., 2016. An ice core derived 1013-year catchment-scale annual rainfall reconstruction in subtropical eastern Australia. Hydrol. Earth Syst. Sci. 20 (5), 1703–1717. https://doi.org/10.5194/hess-20-1703-2016.
Turner, J., 2004. The El Niño–southern oscillation and Antarctica. Int. J. Climatol. 24 (1), 1–31. https://doi.org/10.1002/joc.965.
Turner, S.W.D., Galelli, S., 2016. Regime-shifting streamflow processes: implications for water supply reservoir operations. Water Resour. Res. https://doi.org/10.1002/2015WR017913.
van Dijk, A.I.J.M., Beck, H.E., Crosbie, R.S., de Jeu, R.A.M., Liu, Y.Y., Podger, G.M., Timbal, B., Viney, N.R., 2013. The Millennium Drought in southeast Australia (2001–2009): natural and human causes and implications for water resources, ecosystems, economy, and society. Water Resour. Res. 49 (2), 1040–1057. https://doi.org/10.1002/wrcr.20123.
Van Loon, A.F., 2015. Hydrological drought explained. Wiley Interdiscip. Rev. Water 2 (4), 359–392. https://doi.org/10.1002/wat2.1085.
van Ommen, T.D., Morgan, V., 2010. Snowfall increase in coastal East Antarctica linked with southwest Western Australian drought. Nat. Geosci. 3 (4), 267–272. https://doi.org/10.1038/ngeo761.
Vance, T.R., van Ommen, T.D., Curran, M.A.J., Plummer, C.T., Moy, A.D., 2013. A millennial proxy record of ENSO and Eastern Australian rainfall from the law dome ice core, East Antarctica. J. Clim. 26 (3), 710–725. https://doi.org/10.1175/JCLI-D-12-00003.1.
Vance, T.R., Roberts, J.L., Plummer, C.T., Kiem, A.S., van Ommen, T.D., 2015. Interdecadal Pacific variability and eastern Australian megadroughts over the last millennium. Geophys. Res. Lett. 42 (1), 129–137. https://doi.org/10.1002/2014GL062447.
Vance, T.R., Roberts, J.L., Moy, A.D., Curran, M.A.J., Tozer, C.R., Gallant, A.J.E., Abram, N.J., van Ommen, T.D., Young, D.A., Grima, C., Blankenship, D.D., Siegert, M.J., 2016. Optimal site selection for a high-resolution ice core record in East Antarctica. Clim. Past 12 (3), 595–610. https://doi.org/10.5194/cp-12-595-2016.
Vance, T.R., Roberts, J.L., Plummer, C.T., Kiem, A.S., van Ommen, T.D., 2017. Comment on "Drought variability in the eastern Australia and New Zealand summer drought atlas (ANZDA, CE 1500-2012) modulated by the Interdecadal Pacific Oscillation" by Palmer et al., 2015, doi: 10.1088/1748-9326/10/12/124002. Environ. Res. Lett. 12 (6), 068001. https://doi.org/10.1088/1748-9326/aa7282.
Vaze, J., Jordan, P., Beecham, R., Frost, A., Summerell, G., 2012. Guidelines for rainfall-runoff modelling: towards best practice model application. Report.
Vaze, J., Post, D.A., Chiew, F.H.S., Perraud, J.M., Viney, N.R., Teng, J., 2010. Climate non-stationarity – validity of calibrated rainfall–runoff models for use in climate change studies. J. Hydrol. 394 (3–4), 447–457. https://doi.org/10.1016/j.jhydrol.2010.09.018.
Verdon-Kidd, D.C., Kiem, A.S., 2009. Nature and causes of protracted droughts in southeast Australia: comparison between the Federation, WWII, and Big Dry droughts. Geophys. Res. Lett. 36 (22), L22707. https://doi.org/10.1029/2009gl041067.
Verdon, D.C., Franks, S.W., 2007. Long-term drought risk assessment in the Lachlan River Valley – a paleoclimate perspective. Aust. J. Water Resour. 11 (2), 145–152.
Welhouse, L.J., Lazzara, M.A., Keller, L.M., Tripoli, G.J., Hitchman, M.H., 2016. Composite analysis of the effects of ENSO events on Antarctica. J. Clim. 29 (5), 1797–1808. https://doi.org/10.1175/JCLI-D-15-0108.1.
Westerberg, I.K., Guerrero, J.L., Younger, P.M., Beven, K.J., Seibert, J., Halldin, S., Freer, J.E., Xu, C.Y., 2011. Calibration of hydrological models using flow-duration curves. Hydrol. Earth Syst. Sci. 15 (7), 2205–2227. https://doi.org/10.5194/hess-15-2205-2011.
Wilson, R., Cook, E., D'Arrigo, R., Riedwyl, N., Evans, M.N., Tudhope, A., Allan, R., 2010. Reconstructing ENSO: the influence of method, proxy data, climate forcing and teleconnections. J. Quat. Sci. 25 (1), 62–78. https://doi.org/10.1002/jqs.1297.
Woodhouse, C., Lukas, J., 2006a. Drought, tree rings and water resource management in Colorado. Can. Water Resour. J. 31 (4), 297–310. https://doi.org/10.4296/cwrj3104297.
Woodhouse, C., Lukas, J., 2006b. Multi-century tree-ring reconstructions of Colorado streamflow for water resource planning. Clim. Change 78 (2–4), 293–315. https://doi.org/10.1007/s10584-006-9055-0.
Wooldridge, S.A., Franks, S.W., Kalma, J.D., 2001. Hydrological implications of the Southern Oscillation: variability of the rainfall-runoff relationship. Hydrol. Sci. J. 46 (1), 73–88.
Yang, Y., McVicar, T.R., Donohue, R.J., Zhang, Y., Roderick, M.L., Chiew, F.H.S., Zhang, L., Zhang, J., 2017. Lags in hydrologic recovery following an extreme drought: assessing the roles of climate and catchment characteristics. Water Resour. Res. https://doi.org/10.1002/2017WR020683.
Zambrano Bigiarini, M., 2014. hydroGOF: goodness-of-fit functions for comparison of simulated and observed hydrological time series. R package version 0.3-8, edited.
Zhang, L., Potter, N., Hickel, K., Zhang, Y., Shao, Q., 2008. Water balance modeling over variable time scales based on the Budyko framework – model development and testing. J. Hydrol. 360 (1–4), 117–131. https://doi.org/10.1016/j.jhydrol.2008.07.021.
Zhang, L., Hickel, K., Dawes, W.R., Chiew, F.H.S., Western, A.W., Briggs, P.R., 2004. A rational function approach for estimating mean annual evapotranspiration. Water Resour. Res. 40 (2). https://doi.org/10.1029/2003WR002710.